Politecnico di Milano

V Facoltà di Ingegneria

Corso di laurea in Ingegneria Fisica

Dipartimento di Ingegneria dei Sistemi

Chip to Chip Entanglement Distribution

Supervisor: Prof. R. Osellame, Dr M. Thompson
Co-supervisor: Jianwei Wang

Master Degree by:
Matteo Villa
Matr.804091

Academic Year 2014-2015

Is the moon there when nobody looks?

D. Mermin (and A. Einstein)

Contents

Chapter 1

Introduction

As classical computers rapidly approach the full extent of their power as allowed by the classical laws of physics, quantum information is likely to become one of the most crucial areas of science in the next decades. The groundbreaking work of Bell[1] has opened the way to an incredibly wide world of possibilities, where the classical concept of locality no longer holds. It was only in the last twenty years that physicists and engineers have managed to overcome the daunting technological issue and successfully succeeded in proving experimentally the potential of the quantum properties of matter and light, and even though a full-fledged quantum technology is still a long way to go, fundamental progress have been made[2]. In the last ten years quantum optics has emerged as one of the leading approach to quantum information[3, 4] and quantum communication, since single photons are largely free of noise, can be easily manipulated to create one qubit logic gates and can be encoded in many different degrees of freedom. Although bulk optics was used in the first experimental demonstrations, it has recently been overtaken by integrated quantum optics[5, 6, 7, 8, 9] which offers previously unmatched qualities in terms of stability and scalability, a key point for the realization of, e.g., a quantum computer[10].

In this respect, the possibility of generating, manipulating and transmitting entangled states in a reliable way and with a high visibility is a key passage towards the development of mature quantum technologies, such as large scale quantum networks and quantum cloud computing, but also quantum simulators and computers might greatly benefit from a reliable quantum photonic interconnect. An important requirement for such a device would certainly be the possibility to coherently transmit and convert entangled states within different types of encoding and media. If the generation and the manipulation of entangles states has already been achieved in efficient integrated circuits[11, 12, 13], long distance distribution of entangled states

1

has been demonstrated[14, 15, 16], both in fibre and free space, only by means of network nodes relying on bulk optical components, which suffer of non-scalability and stability problems. In this thesis we report a high fidelity demonstration of entanglement distribution between two integrated Silicon on Insulator (SoI) chips connected with an optical fibre, by means of a coherent interconversion between path encoding, on chip, and polarization encoding, more suitable for free space and fibre propagation.

Chapter 2

Theoretical Background

The purpose of this chapter is to review those topics of quantum optics and quantum information which are most relevant to this thesis. I shall therefore introduce the notation and the key equations which I will use from here on. It is not meant to be a complete or accurate description and a prior knowledge of quantum mechanics is assumed. Nevertheless, I will try to be rigorous and demonstrate in detail all the results which will play a significant part in the following sections.

2.1 Elements of Quantum Information

In this section we review some basic concepts of quantum information [17, 18], focusing our analysis to the topic of one qubit arbitrary operation, as it is most significant in our work. Regardless of how it is physically realized, a quantum bit of information, a *qubit*, is represented by a ket vector as follows:

$$|0\rangle = \begin{pmatrix} 1 \\ 0 \end{pmatrix} \quad |1\rangle = \begin{pmatrix} 0 \\ 1 \end{pmatrix} \tag{2.1}$$

The vector notation is necessary since qubits, unlike classical bits, are not constrained to be either $|0\rangle$ or $|1\rangle$ but can be in a superposition of these two:

$$|\psi\rangle = a\,|0\rangle + b\,|1\rangle = \begin{pmatrix} a \\ b \end{pmatrix} \tag{2.2}$$

where $a, b \in \mathbb{C}$ with the requirement:

$$|a|^2 + |b|^2 = 1 \tag{2.3}$$

A useful and very popular way to visualize qubits is by drawing unit vectors on a sphere called the Bloch sphere. We can see why if we rewrite the coefficients a, b in Cartesian or polar coordinates:

$$a = x_a + iy_a = r_a e^{i\phi_a}$$
$$b = x_b + iy_b = r_b e^{i\phi_b}$$

(2.4)

one of the two phase is redundant:

$$|\psi\rangle = x_a + iy_a \,|0\rangle + x_b + iy_b \,|1\rangle$$
$$= r_a e^{i\phi_a} \,|0\rangle + r_b e^{i\phi_b} \,|1\rangle = r_a \,|0\rangle + r_b e^{i(\phi_b - \phi_a)} \,|1\rangle$$

(2.5)

since we can drop the global phase as it has no observable consequence. If we switch back to the Cartesian coordinates for b, and consider the normalization condition:

$$|r_a|^2 + |x + iy|^2 = r_a^2 + x^2 + y^2 = 1$$

(2.6)

which is just the equation fo a sphere. If we switch to polar coordinates:

$$x = \sin(\theta)\cos(\phi)$$
$$y = \sin(\theta)\sin(\phi)$$
$$r_a = z = \cos(\theta)$$

(2.7)

We can now easily write:

$$|\psi\rangle = z\,|0\rangle + (x + iy)\,|1\rangle$$
$$= \cos(\theta)\,|0\rangle + \sin(\theta)\,(\cos(\phi) + i\sin(\phi))\,|1\rangle$$
$$= \cos(\theta)\,|0\rangle + \sin(\theta)e^{i(\phi)}\,|1\rangle$$

(2.8)

But we want to map the different possible qubit states to a full sphere (right now $|0\rangle$ and $|1\rangle$ differ for a 90° change in θ) and we thus make the substitution $\theta' = 2\theta$:

$$|\psi\rangle = \cos(\frac{\theta}{2})\,|0\rangle + \sin(\frac{\theta}{2})e^{i\phi}\,|1\rangle$$

(2.9)

where we dropped the prime index for convenience. As a result of the construction of the Bloch sphere, orthogonal states are represented by antipodal points on the Bloch sphere.

We now turn our attention to the description of quantum gates. Since we must implement a quantum gate as the evolution of an isolated quantum system, the transformation is governed by the Schroedinger equation:

$$i\hbar \frac{\partial \psi}{\partial t} = H\psi \tag{2.10}$$

The formal solution is of the form:

$$\psi(t) = \exp\left(\frac{-iH}{\hbar}\right)\psi(0) = U\psi(0) \tag{2.11}$$

where U is just a unitary matrix. Once again, we can forget about the physical process, which is buried within H, and study the evolution of a state in terms of unitary matrix, whose action is always logically reversible. The first quantum gates we want to study are those acting on a single qubit, or 1-Qubit Gates. We start then fro the Pauli matrices, which are of particular interest since any 1-qubit gate can be written as a weighted sum of these matrices:

$$I = \begin{pmatrix} 1 & 0 \\ 0 & 1 \end{pmatrix} \quad X = \begin{pmatrix} 0 & 1 \\ 1 & 0 \end{pmatrix} \quad Y = \begin{pmatrix} 0 & -i \\ i & 0 \end{pmatrix} \quad Z = \begin{pmatrix} 1 & 0 \\ 0 & -1 \end{pmatrix} \tag{2.12}$$

As an example, we show how the X acts on the qubits $|0\rangle$ and $|1\rangle$.

$$X|0\rangle = \begin{pmatrix} 0 & 1 \\ 1 & 0 \end{pmatrix} \cdot \begin{pmatrix} 1 \\ 0 \end{pmatrix} = \begin{pmatrix} 0 \\ 1 \end{pmatrix} = |1\rangle$$

$$X|1\rangle = \begin{pmatrix} 0 & 1 \\ 1 & 0 \end{pmatrix} \cdot \begin{pmatrix} 0 \\ 1 \end{pmatrix} = \begin{pmatrix} 1 \\ 0 \end{pmatrix} = |0\rangle \tag{2.13}$$

The Pauli X matrix is just the classical reversible NOT, although it is not a universal gate, that is, it does only map the North pole of the Bloch sphere to the South pole, but it does not map a generic qubit to its antipodal state. We now show how to write any single qubit density operator in terms of the Pauli matrix. Starting from equation (2.9) we compute the density matrix of a generic pure state:

$$\rho = \begin{pmatrix} \cos(\frac{\theta}{2}) \\ e^{i\phi}\sin(\frac{\theta}{2}) \end{pmatrix} \cdot \begin{pmatrix} \cos(\frac{\theta}{2}) & e^{-i\phi}\sin(\frac{\theta}{2}) \end{pmatrix} = \begin{pmatrix} \cos^2(\frac{\theta}{2}) & e^{-i\phi}\sin(\frac{\theta}{2})\cos(\frac{\theta}{2}) \\ e^{i\phi}\sin(\frac{\theta}{2})\cos(\frac{\theta}{2}) & \sin^2(\frac{\theta}{2}) \end{pmatrix}$$

$$= \frac{1}{2}\begin{pmatrix} 1+\cos(\theta) & e^{-i\phi}\sin(\theta) \\ e^{i\phi}\sin(\theta) & 1-\cos(\theta) \end{pmatrix} = \frac{1}{2}\left(I + \sin(\theta)\cos(\phi)X + \sin(\theta)\sin(\phi)Y + \cos(\theta)Z\right)$$

We can rewrite this last expression in a compact way by defining:

$$\vec{n} = (\sin(\theta)\cos(\phi), \sin(\theta)\sin(\phi), \cos(\theta)) \tag{2.14}$$

Therefore:

$$\rho = \frac{1}{2}(1 + \vec{\sigma} \cdot \vec{n}) \tag{2.15}$$

Another important single qubit gate is the Hadamard gate. The Hadamard, or H gate, is defined by the matrix:

$$H = \frac{1}{\sqrt{2}}\begin{pmatrix} 1 & 1 \\ 1 & -1 \end{pmatrix} \tag{2.16}$$

and its action on the $|0\rangle$ and $|1\rangle$ qubit is:

$$
\begin{aligned}
H|0\rangle &= \frac{1}{\sqrt{2}}(|0\rangle + |1\rangle) \\
H|1\rangle &= \frac{1}{\sqrt{2}}(|0\rangle - |1\rangle)
\end{aligned} \tag{2.17}
$$

and conversely:

$$
\begin{aligned}
H\frac{1}{\sqrt{2}}(|0\rangle + |1\rangle) &= |0\rangle \\
H\frac{1}{\sqrt{2}}(|0\rangle - |1\rangle) &= |1\rangle
\end{aligned} \tag{2.18}
$$

How can we write an arbitrary single qubit unitary operation, possibly in terms of the Pauli matrices? If we consider the Bloch sphere, we can define a rotation around an axis in the following way:

$$R_x = \exp\left(-i\theta\frac{X}{2}\right) = \cos\left(\frac{\theta}{2}\right)I - i\sin\left(\frac{\theta}{2}\right)X = \begin{pmatrix} \cos(\frac{\theta}{2}) & -i\sin(\frac{\theta}{2}) \\ -i\sin(\frac{\theta}{2}) & \cos(\frac{\theta}{2}) \end{pmatrix}$$

$$R_y \equiv \exp\left(-i\theta\frac{Y}{2}\right) = \cos\left(\frac{\theta}{2}\right)I - i\sin\left(\frac{\theta}{2}\right)Y = \begin{pmatrix} \cos(\frac{\theta}{2}) & -\sin(\frac{\theta}{2}) \\ \sin(\frac{\theta}{2}) & \cos(\frac{\theta}{2}) \end{pmatrix}$$

$$R_z \equiv \exp\left(-i\theta\frac{Z}{2}\right) = \cos\left(\frac{\theta}{2}\right)I - i\sin\left(\frac{\theta}{2}\right)Z = \begin{pmatrix} e^{(-i\frac{\theta}{2})} & 0 \\ 0 & e^{(i\frac{\theta}{2})} \end{pmatrix}$$

Which we can further generalize as a rotation around a generic real unit vector $\hat{n} = (n_x, n_y, n_z)$ as follows:

$$R_{\hat{n}} \equiv \exp\left(-i\theta\hat{n} \cdot \vec{\sigma}\right) = \cos\left(\frac{\theta}{2}\right) I - i \sin\left(\frac{\theta}{2}\right) \hat{n} \cdot \vec{\sigma} \qquad (2.19)$$

Now, a generic 2×2 unitary matrix U must have the module of its determinant unitary, i.e. $|det(U)| = 1$. If $det(U) = 1$ the matrix is said to be special unitary. we can always decompose a generic unitary in terms of a special unitary times a phase shift as follows:

$$U = e^{i\delta}V = e^{i\delta} \begin{pmatrix} 1 & 0 \\ 0 & 1 \end{pmatrix} V = Ph(\delta) \cdot V \qquad (2.20)$$

It is possible to show that an equivalent condition to being unitary is that rows and columns must be orthogonal. Therefore, without loss of generality, we can write:

$$V = \begin{pmatrix} \alpha & -\beta^* \\ \beta & \alpha^* \end{pmatrix} \qquad (2.21)$$

with α and β are complex number that satisfy $|\alpha|^2 + |\beta|^2 = 1$. A convenient choice for α and β is the following:

$$\alpha = e^{i\mu} \cos(\frac{\theta}{2}) \quad \beta = e^{i\xi} \sin(\frac{\theta}{2}) \qquad (2.22)$$

so that

$$V = \begin{pmatrix} e^{i\mu} \cos(\frac{\theta}{2}) & -e^{-i\xi} \sin(\frac{\theta}{2}) \\ e^{i\xi} \sin(\frac{\theta}{2}) & e^{-i\mu} \cos(\frac{\theta}{2}) \end{pmatrix} \qquad (2.23)$$

But we can easily obtain this as product of the following three rotations:

$$R_z(\xi - \mu) \cdot R_y(\theta) \cdot R_z(-\xi - \mu) \qquad (2.24)$$

As it is straightforward to verify by applying the definition of the axis rotation. Therefore a unitary 1-qubit gate can be decomposed into the form:

$$U = Ph(\delta) \cdot R_z(\xi - \mu) \cdot R_y(\theta) \cdot R_z(-\xi - \mu) \qquad (2.25)$$

The reason why an arbitrary rotation can be expressed without a R_x is soon explained if we consider the following expansion:

$$R_x(\theta) = \exp\left(-i\theta\frac{X}{2}\right) = R_z(-\frac{\pi}{2}) \cdot R_y(\theta) \cdot R_z(\frac{\pi}{2}) = R_y(\frac{\pi}{2}) \cdot R_y(\theta) \cdot R_z(-\frac{\pi}{2})$$

The results we proved in this section will be extremely useful, since we will be able to express the action of the integrated Mach-Zehnder (plus a phase shifter) on a qubit in terms of the Pauli matrices and the Hadamard gate.

2.2   Quantum Optics of the Beam Splitter

The beam splitter is one of the building blocks of every quantum circuit[19] and is very useful for splitting single photons or bright light into different paths, while the most interesting features are the possibility to interfere quantum states of light[20, 21], using Mach Zehnder-like structures, or to create path entangled states (or NOON state in general).
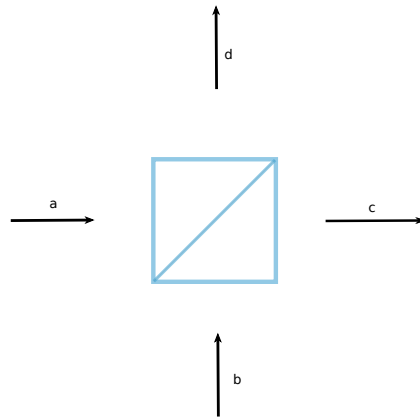

Figure 2.1: Scheme of a generic Beam Splitter.

The boundary conditions at surface of the beam splitter lead to the relations:

$$c = ta + rb$$
$$d = ra + tb$$

(2.26)

with

$$|t^2| + |r^2| = 1$$
$$rt^* + r^*t = 0$$

(2.27)

where the conditions on t and r directly come from the conservation of energy (the beam splitter is supposed to be lossless). It is worth noting that

we are considering an Heisenberg picture as we are propagating the operators. Since in all practical cases we want to input a certain known state and then calculate the output in this fashion:

$$|\Psi_{out}\rangle = U |\Psi_{in}\rangle \tag{2.28}$$

the Schroedinger picture is more natural. The form of U can be calculated explicitly, but since the equations (2.26) have the form of a rotation and one can show that the rotation operator:

$$U = \exp\left[i\theta \left(a^\dagger b + b^\dagger a\right)\right] \tag{2.29}$$

We want to show now how to obtain the equations (2.26) by computing the expression $c = U^\dagger a U$, which is instead the Heisenberg Picture, in order to connect the two different representations. This is done by means of a Taylor expansion of the exponential matrix U. A generic expression for this expansion is:

$$\begin{aligned}
\exp(-\lambda A) & B \exp(-\lambda A) = \\
&= (I - \lambda A + \frac{1}{2}\lambda^2 A + \ldots)B(I + \lambda A + \frac{1}{2}\lambda^2 A + \ldots) \\
&= B - \lambda\left[A, B\right] + \frac{1}{2}\lambda^2\left[A, \left[A, B\right]\right] \\
&+ \frac{1}{3!}\lambda^3\left[A, \left[A, \left[A, B\right]\right]\right]
\end{aligned} \tag{2.30}$$

where $\lambda \in \mathbb{C}$ and A, B are two generic analytical operators. We apply this expansion to $c = U^\dagger a U$:

$$\begin{aligned}
c = U^\dagger a U &= \exp\left[-i\theta\left(a^\dagger b + b^\dagger a\right)\right]a\exp\left[i\theta\left(a^\dagger b + b^\dagger a\right)\right] \\
&= a - \theta b - \frac{1}{2}|\theta|^2 a + \frac{1}{3}\theta|\theta|^2 b + \ldots \\
&= a\cos(|\theta|) - e^{i\phi_\theta}\sin(|\theta|)
\end{aligned} \tag{2.31}$$

Due to the conditions set by (2.26), we can choose the phase arbitrarily, and a convenient choice is $\phi_\theta = -\frac{\pi}{2}$. This way we can write, after a similar process for $d = U^\dagger b U$:

$$\begin{aligned}
c = U^\dagger a U &= \cos\left(\theta\right)a + i\sin\left(\theta\right)b \\
d = U^\dagger b U &= i\sin\left(\theta\right)a + \cos\left(\theta\right)b
\end{aligned} \tag{2.32}$$

As we will see later, we are interested in writing the input operators a, b in terms of the output c, d. We must therefore consider the inverse transformation, which, for the creation operators, looks like:

$$Ua^\dagger U^\dagger = \cos\left(\theta\right) a^\dagger + i\sin\left(\theta\right) b^\dagger = \cos\left(\theta\right) c^\dagger + i\sin\left(\theta\right) d^\dagger \qquad (2.33)$$

$$Ub^\dagger U^\dagger = i\sin\left(\theta\right) a^\dagger + \cos\left(\theta\right) b^\dagger = i\sin\left(\theta\right) c^\dagger + \cos\left(\theta\right) d^\dagger \qquad (2.34)$$

Where the last equality in both lines follows from the fact that, in the Schroedinger picture, the operators do not evolve. If $\cos\left(\theta\right) = \sin\left(\theta\right) = \frac{1}{\sqrt{2}}$ the beam splitter is called balanced. The condition to obtain this state depends on the physical realization of the beam splitter. Typically, in integrated optics, this is done by means of directional couplers or MMIs. We can now consider what happens when we input a single photon in one arm of the beam splitter, that is when we input the state:

$$\left|\Psi_{in}\right\rangle = \left|1_a\right\rangle \left|0_b\right\rangle \qquad (2.35)$$

We can now use the formalism we developed before as follows:

$$\begin{aligned}
\left|\psi_{out}\right\rangle &= U\left|1_a\right\rangle \left|0_b\right\rangle = Ua^\dagger \left|0_a\right\rangle \left|0_b\right\rangle = Ua^\dagger U^\dagger U \left|0_a\right\rangle \left|0_b\right\rangle \\
&= \left(rc^\dagger + itd^\dagger\right) \left|0_c\right\rangle \left|0_d\right\rangle = r\left|1_c\right\rangle \left|0_d\right\rangle + it\left|0_c\right\rangle \left|1_d\right\rangle
\end{aligned} \qquad (2.36)$$

We can see that the single photon exits from either one or the other arm of the beam splitter with probabilities proportional to r, t. So far the Quantum description agrees with the classical one. In order to see any difference we must inspect in closer detail Quantum Interference, which is the subject of the next section.

2.3   Quantum Interference

2.3.1   Hong-Ou-Mandel Dip

We will now see how multimode fields lead to features which can be explained only in terms of quantum interference of single photons. The simplest and most famous case is the Hong-Ou-Mandel dip[22, 23]. Let us consider a single photon input for each arm of the beam splitter as in figure. We start by considering two completely distinguishable single photons (that is two photons which are in two different modes, besides the spatial one), so that the input state is in the form:

$$|\Psi_{in}\rangle = |11\rangle = a_{\omega 1}^\dagger b_{\omega 2}^\dagger |0\rangle\rangle \tag{2.37}$$

$$
\begin{aligned}
|\psi_{out}\rangle &= U a_{\omega 1}^\dagger b_{\omega 2}^\dagger |0\rangle\rangle = U a_{\omega 1}^\dagger U^\dagger U b_{\omega 2}^\dagger U^\dagger |0\rangle\rangle \\
&= \left(r c_{\omega 1}^\dagger + i t d_{\omega 1}^\dagger \right) \left(+ i t c_{\omega 2}^\dagger + r d_{\omega 2}^\dagger \right) |0\rangle\rangle \\
&= \left[i r t \left(c_{\omega 1}^\dagger c_{\omega 2}^\dagger + d_{\omega 1}^\dagger d_{\omega 2}^\dagger \right) + r^2 c_{\omega 1}^\dagger d_{\omega 2}^\dagger - t^2 c_{\omega 2}^\dagger d_{\omega 1}^\dagger \right] |0\rangle\rangle \\
&= i r t \left(|1100\rangle + |0011\rangle \right) + r^2 |1001\rangle - t^2 |0110\rangle
\end{aligned} \tag{2.38}
$$

If we now put a detector at the end of each arm of the beam splitter and look for the probability of obtaining a coincidence count we find:

$$P_{cc}^{dist} = r^4 + t^4 = R^2 + \left(1 - R^2 \right) \tag{2.39}$$

where $R = r^2$ is the reflectivity of the beam splitter. If we consider $R = \frac{1}{2}$, then $P_{cc}^{dist} = \frac{1}{2}$, in perfect agreement with a fully probabilistic description where the photon is half of the time transmitted and half reflected. A completely different result is obtained if the two photons are indistinguishable as we now show following almost exactly the same reasoning above. The input state this time is of the form:

$$|\Psi_{in}\rangle = |11\rangle = a^\dagger b^\dagger |0_a\rangle |0_b\rangle \tag{2.40}$$

Thus, after the beam splitter we get:

$$
\begin{aligned}
|\psi_{out}\rangle &= U |1_a\rangle |1_b\rangle = U a^\dagger b^\dagger |0_a\rangle |0_b\rangle = U a^\dagger U^\dagger U b^\dagger U^\dagger |0_a\rangle |0_b\rangle \\
&= \frac{1}{2} \left(r c^\dagger + i t d^\dagger \right) \left(+ i t c^\dagger + r d^\dagger \right) |0_c\rangle |0_d\rangle \\
&= i r t \sqrt{2} \left(|2_c\rangle |0_d\rangle + |0_c\rangle |2_d\rangle \right) + \left(r^2 - t^2 \right) |1_c 1_d\rangle
\end{aligned} \tag{2.41}
$$

If we now evaluate the probability to obtain a coincidence count:

$$P_{cc}^{dist} = \left(r^2 - t^2 \right)^2 = \left(1 - 2R \right)^2 \tag{2.42}$$

If the beam splitter is balanced, the probability P_{cc}^{indist} vanishes. This result, which is highly non classical, reflects the bosonic nature of photons. The output state is therefore:

$$|\psi_{out}\rangle = \frac{i}{\sqrt{2}} \left(|2_c\rangle |0_d\rangle + |0_c\rangle |2_d\rangle \right) \tag{2.43}$$

The beam splitter is therefore a key component to erase the "which path" information and the output state is just a path entangled quantum state.
A useful parameter[19] to characterize the quality of the interference is the visibility, defined as:

$$V = 1 - \frac{P_{cc}^{indist}}{P_{cc}^{dist}} \tag{2.44}$$

which, in the case where the photons are indistinguishable in all other degrees of freedom, is limited by the reflectivity R as follows:

$$V = 1 - \frac{(1 - 2R)^2}{R^2 + (1 - R)^2} \tag{2.45}$$

As we can see from the Figure 2.2 the visibility of the fringes is very robust to variations of the reflectivity R from 0.5. A reflectivity of $R = 0.51$ (which is a typical fabrication tolerance for MMIs coupler, see next chapter) results in fringes with a visibility $V = 0.9992$.
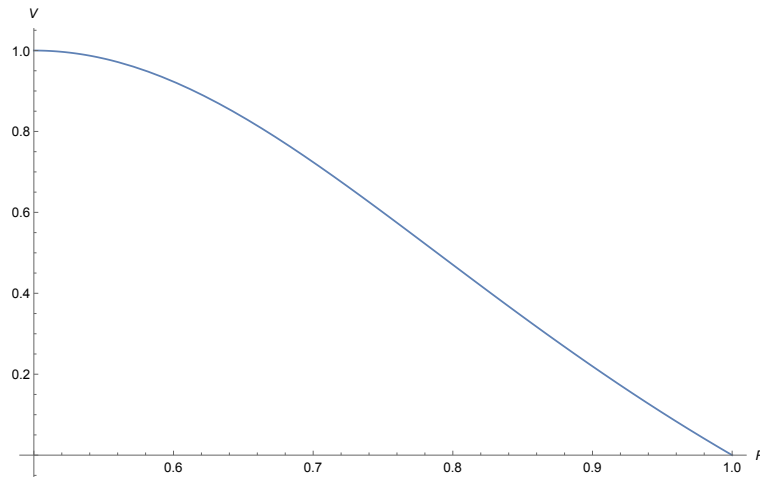

Figure 2.2: Visibility of the quantum fringes as a function of the reflectivity of the beam splitter.
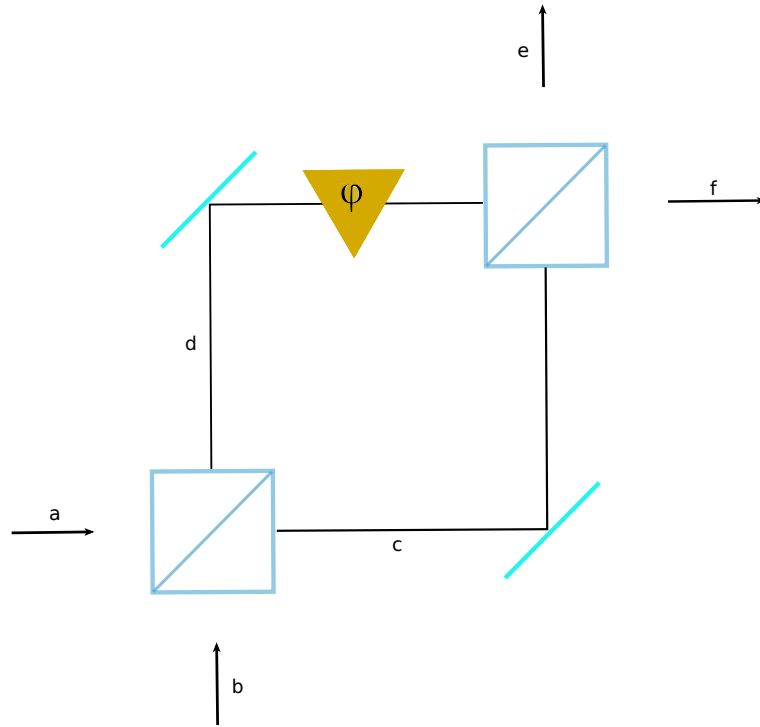
Figure 2.3: Schematic of an MZI. The beam splitters are usually balanced.

2.3.2 Mach-Zehnder Interferometer

We now turn our attention to a slightly more involved structure: a Mach-Zender interferometer (MZI). As it apparent from the figure a MZI is just a series of two beam splitters, with the addition of a phase shifter on one of the two outputs after the first beam splitter.

We firstly consider a single photon input (we use the Heisenberg Picture because is somewhat more practical in this case), thus, if we consider the phase shifter matrix in the form:

$$\varphi = \begin{pmatrix} 1 & 0 \\ 0 & e^{-i\varphi} \end{pmatrix} \tag{2.46}$$

Then the input evolves as follows (we directly consider balanced beam splitters):

$$|\psi_{in}\rangle = |1_a\rangle\,|0_b\rangle$$

$$\xrightarrow{BS1} \frac{\left(c^\dagger + id^\dagger\right)}{\sqrt{2}}\,|0_c\rangle\,|0_d\rangle = \frac{1}{\sqrt{2}}\,|1_c\rangle\,|0_d\rangle + i\,|0_c\rangle\,|1_d\rangle$$

$$\xrightarrow{\varphi} \frac{1}{\sqrt{2}}\,|1_c\rangle\,|0_d\rangle + ie^{-i\varphi}\,|0_c\rangle\,|1_d\rangle \tag{2.47}$$

$$\xrightarrow{BS2} \frac{1}{2}\left[\left(1 - e^{-i\varphi}\right)|1_e\rangle\,|0_f\rangle + i\left(1 + e^{-i\varphi}\right)|0_e\rangle\,|1_f\rangle\right]$$

So that the probabilities of obtaining on detector e, f are, respectively, $P_e = \frac{1}{2}\left(1 - \cos(\varphi)\right)$ and $P_e = \frac{1}{2}\left(1 + \cos(\varphi)\right)$. As we might expect from the beam splitter analysis, this can still be seen as a classical interference, as the detection probability will oscillate sinusoidally with phase φ. On the other hand, if we do not aim to prove the quantum nature of light, we can regard the MZI to create the following superposition of states:

$$|10\rangle \to \cos(\frac{\varphi}{2})\,|10\rangle + i\sin(\frac{\varphi}{2})\,|01\rangle \tag{2.48}$$

We now turn our attention to the case the input of the first beam splitter is the state:

$$|\Psi_{in}\rangle = |1_a\rangle\,|1_b\rangle \tag{2.49}$$

where the photons are completely indistinguishable (as usual, aside from the spatial mode). Following the same calculations of the single input state:

$$|\psi_{in}\rangle = |1_a\rangle\,|1_b\rangle$$

$$\xrightarrow{BS1} \frac{\left(c^\dagger + id^\dagger\right)}{\sqrt{2}}\frac{\left(c^\dagger + id^\dagger\right)}{\sqrt{2}}\,|0_c\rangle\,|0_d\rangle = \frac{i}{\sqrt{2}}\,|2_c\rangle\,|0_d\rangle + |0_c\rangle\,|2_d\rangle$$

$$\xrightarrow{\varphi} \frac{i}{\sqrt{2}}\,|2_c\rangle\,|0_d\rangle + e^{-i2\varphi}\,|0_c\rangle\,|2_d\rangle$$

$$\xrightarrow{BS2} i\left[\frac{\left(1 - e^{-i2\varphi}\right)}{2}\left(\frac{|2_e\rangle\,|0_f\rangle - |0_e\rangle\,|2_f\rangle}{\sqrt{2}}\right) + i\frac{\left(1 + e^{-i2\varphi}\right)}{2}\,|1_e\rangle\,|1_f\rangle\right] \tag{2.50}$$

If we now drop a global phase factor we get:

$$|\psi_{out}\rangle = \sin(\varphi)\left(\frac{|2_e\rangle\,|0_f\rangle - |0_e\rangle\,|2_f\rangle}{\sqrt{2}}\right) + \cos(\varphi)\,|1_e\rangle\,|1_f\rangle \tag{2.51}$$

It is suggestive to rewrite the last equation as:

$$|\psi_{out}\rangle = \sin(\varphi)\,|\psi_{bunch}\rangle + \cos(\varphi)\,|\psi_{antibunch}\rangle \qquad (2.52)$$

This shows clearly that, by changing the phase φ, we can control whether the output photons will bunch together in one of the two different paths, or will split. By recording the coincidence counts, we will see a fringe with half the period if compared to the single photon case (which is also the case for classical light, e.g. a bright laser beam). We could have also computed all the preceding calculations by computing the Mach-Zehnder matrix:

$$MZI = BS \cdot Ph(\phi) \cdot BS = \begin{pmatrix} \sin(\frac{\varphi}{2}) & \cos(\frac{\varphi}{2}) \\ \cos(\frac{\varphi}{2}) & -\sin(\frac{\varphi}{2}) \end{pmatrix} \qquad (2.53)$$

where we dropped a global unobservable phase factor in the last inequality.
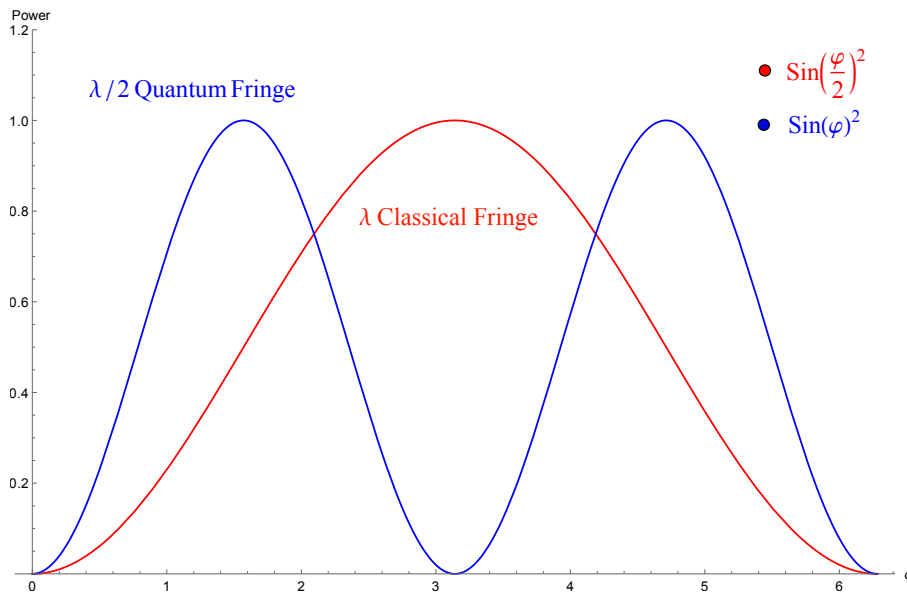

Figure 2.4: Classical and Quantum Interference.

2.4   Bell's Theorem

In 1935 Einstein, Podolsky and Rosenberg published a paper[24] entitled "Can Quantum Mechanical Description of Reality Be Considered Complete?",

where they put under close investigation the assumptions of quantum mechanics. In their opinion, a physicist must ask himself two questions while evaluating if a physical theory is valid or not:

1. Is the theory correct?

2. Is the description given by the theory complete?

In order to answer these questions in a precise way, they reckoned it was necessary to better define two concepts, completeness and reality. They gave the following definitions:

1. Complete: A theory can be considered complete only if every element of physical reality has a counterpart in the theory.

2. Reality: If, without anyway of disturbing a system, we can predict with certainty (i.e. with probability equal to one) the value of a physical quantity, then there exist an element of physical reality corresponding to this physical quantity.

They regarded the first condition as a necessary one, while the second is (obviously) only sufficient, but the considered it general enough to suffice for their argument. With simple quantum mechanical considerations, they then showed that, by considering an entangled state of two systems of the form:

$$\Psi\left(x_1, x_2\right) = \sum_{i=1}^{\infty} \phi\left(x_1\right) \upsilon\left(x_2\right) \tag{2.54}$$

one can predict with certainty the value of a physical quantity of the second system only by measuring that quantity on the first system but without interacting in anyway with the second. Following their second definition, the measured quantity is therefore an element of reality. Moreover we can imagine to measure the momentum P and the position Q of this entangled state. Both this measurements will allow us to make predictions on the second systems and therefore correspond to elements of reality. But Q and P are non commuting operators that is:

$$[P, Q] = PQ - QP = \frac{h}{2\pi i} \tag{2.55}$$

and quantum mechanics cannot predict the simultaneous values of both these operators. The theory has not a counterpart for every element of reality and thus it is not complete. The loophole in this reasoning is well-expressed in the words of the authors:

> *" Indeed, one would not arrive at our conclusion if one insisted*
> *that two or more physical quantities can be regarded as simulta-*
> *neous elements of reality only when they can be simultaneously*
> *measured or predicted. On this point of view, since either one or*
> *the other, but not both simultaneously of the quantities P and Q*
> *can be predicted, they are not simultaneously real. This makes*
> *the reality of P and Q depend upon the process of measurement*
> *carried out on the first system, which does not disturb the second*
> *system in any way. No reasonable definition of reality could be*
> *expected to permit this".*

It is important to underline that the goal of this paper was not to prove that quantum mechanics was wrong, but merely that it was an incomplete theory. Moreover, there was no apparent disagreement on the correlations predicted by the EPR Gedanken experiment and the debate on the reality of Quantum Mechanics was only an epistemological one that could not easily be disproved by experiments. The situation changed only thirty years later when J. Bell published his paper[1] "On the Einstein Podolsky Rosen Paradox". In his paper, which was later defined as one of the most profound discoveries of the century, Bell proposed a slightly modified EPR experiment that predicted different results for Einstein's point of view, "local realism", and quantum mechanics. The issue was no longer a matter of philosophy, but a very quantitative one which could be answered experimentally. We will now illustrate a simple argument, where we rely heavily on [17], to understand the nature of the problem before addressing it in a more rigorous way, following the approach [25] described by Clauser, Horne, Shimony, Holt (CHSH).

We imagine to prepare two particles and then to send one to Bob and one to Alice. It does not matter the way we prepare our particle, we must only be able to repeat the experimental procedure with which we prepare the particles. We now imagine that Alice has two different measurement apparatuses with which she can measure either P_Q or P_R, which are two different properties of the particle. She does not know in advance what she will be measuring, instead she has a random process to decide between the two possible measurements when she receives the particles. Let the outcome of the P_Q and P_R be Q and R and furthermore let us assume for simplicity that the outcome can only be +1 or -1. The same will be true for Bob's particle and we will call P_S and P_T, while S and T will be the outcome. Alice and Bob will perform the measurement in the same time, so that no physical signal propagating from Alice can influence Bob, as it is evident

from relativistic arguments. If we now consider the quantity:

$$QS + RS + RT - QT = S(R + Q) + T(R - Q) \tag{2.56}$$

it is easy to see that since $Q, R = \pm 1$, then either $S(R + Q) = 0$ or $T(R - Q) = 0$. Therefore

$$QS + RS + RT - QT = \pm 2 \tag{2.57}$$

Suppose next that, before the measurement, the system is in the state where $Q = q, R = r, S = s$ and $T = t$. We can now write the expectation value of the quantity above as:

$$
\begin{aligned}
E(QS + RS + RT - QT) &= \sum_{q,r,s,t} p(q,r,s,t)(qs + rs + rt - qt) \\
&\leq \sum_{q,r,s,t} p(q,r,s,t) \cdot 2 = 2
\end{aligned}
\tag{2.58}
$$

Moreover one can write:

$$
\begin{aligned}
E(QS + RS + RT - QT) &= \sum_{q,r,s,t} p(q,r,s,t)\, qs + \sum_{q,r,s,t} p(q,r,s,t)\, rs \\
&\qquad \sum_{q,r,s,t} p(q,r,s,t)\, rt - \sum_{q,r,s,t} p(q,r,s,t)\, qt \\
&= E(QS) + E(RS) + E(RT) - E(QT)
\end{aligned}
\tag{2.59}
$$

Comparing the two equations above we finally get the Bell's inequality:

$$E(QS) + E(RS) + E(RT) - E(QT) \leq 2 \tag{2.60}$$

We now put quantum mechanics back into the picture by supposing that we prepare two qubits in an entangled state of the type:

$$|\psi\rangle = \frac{|01\rangle - |10\rangle}{\sqrt{2}} \tag{2.61}$$

We then send one qubit to Alice, one to Bob. Assume they perform the following measurements:

$$Q = Z_1 \qquad S = \frac{-Z_2 - X_2}{\sqrt{2}}$$
$$Q = X_1 \qquad T = \frac{Z_2 - X_2}{\sqrt{2}} \tag{2.62}$$

If we calculate the quantum mechanical expectation value of the operators which appear in the Bell's inequality found before we find:

$$\langle QS \rangle = \frac{1}{\sqrt{2}} \quad \langle RS \rangle = \frac{1}{\sqrt{2}} \quad \langle RT \rangle = \frac{1}{\sqrt{2}} \quad \langle QT \rangle = -\frac{1}{\sqrt{2}} \tag{2.63}$$

Thus we easily find:

$$\langle QS \rangle + \langle RS \rangle + \langle RT \rangle - \langle QT \rangle = 2\sqrt{2} \tag{2.64}$$

We now face an apparent paradox: quantum mechanics predicts an experiment results to be in striking disagreement with the Bell's inequality. But which are the assumptions of our first derivation that are not compatible with the picture quantum mechanics gives us of nature? There are at least two:

1. The assumption that the physical properties P_Q, P_R, P_S, P_T have definite values Q, R, S, T which exist independent of observation. This is sometimes known as the assumption of realism.

2. The assumption that Alice performing her measurement does not influence the result of Bob's measurement. This is sometimes known as the assumption of locality

Together this two assumptions are known as *local realism*. We can now perform an experiment of the type described above and based on the result of the Bell's inequality decide whether quantum mechanics is right or not. This has been done with in order to satisfy strict relativist requirements and the results were found to violate Bell's inequality by 30 standard deviations[26]. Although some loopholes remain, it is difficult to expect a completely different outcome from more sophisticated experiments.

2.5   CHSH's Inequality

We will now show a more formal derivation[25, 27] of the CHSH's Inequality derived before. We start by considering an ensemble of correlated pairs of

particle moving towards two different apparatus I_a and II_b, where a, b are adjustable parameters for each setup. In each apparatus the particle can choose between two channels, labeled respectively +1 and -1. Let the result of this selection be $A(a)$ and $B(b)$ which, according to which channel is selected, will have value +1 or -1. We now suppose that a statistical correlation of $A(a)$ and $B(b)$ is due to information carried by and localized within each particle. This information, which is not quantum mechanical, is part of a set of hidden variables which are usually denoted by λ. One can assume that the two particles were in contact some time in the past and could therefore exchange communication regarding this hidden variable. It is a matter of indifference for this argument whether λ is a single variable, a set or even a set of functions and whether this variables are discrete or continuous. We shall therefore follow the standard derivations which assume λ to be a single continuous variable. The correlations one might find are now consequence of the deterministic functions $A(a, \lambda)$ and $B(b, \lambda)$.

The key assumption we know make is that $A(a, \lambda)$ and $B(b, \lambda)$ are independent of b and a respectively. This seems to be a natural consequence of locality, since the experimental apparatus which perform the measurements can be so far apart that, due to relativistic arguments, no signal from one apparatus can physically influence the other one. The second key assumption we make is that the probability distribution of the ensemble, which I will call $\rho(\lambda)$ is independent of both a, b since this two variables can be chosen when the correlated pair is non longer in contact and therefore no longer in condition to exchange information.

We can now define the correlation distribution as:

$$P(a, b) = \int \rho(\lambda) A(a, \lambda) B(b, \lambda) d\lambda \qquad (2.65)$$

with $|A(a, \lambda)|, |B(b, \lambda)| \leq 1$. Now if a, a' and b, b' are different settings for the experimental apparatus, we can write:

$$P(a, b) - P(a, b') = \int \rho(\lambda) \left(A(a, \lambda) B(b, \lambda) - A(a, \lambda) B(b', \lambda) \right) d\lambda \qquad (2.66)$$

If we now add and subtract the quantity $A(a, \lambda) A(a', \lambda) B(b', \lambda) B(b, \lambda)$ to the rhs of the equation:

$$P(a, b) - P(a, b') = \int \rho(\lambda) A(a, \lambda) B(b, \lambda) \left(1 \pm A(a', \lambda) B(b', \lambda) \right) d\lambda \qquad (2.67)$$

$$- \int \rho(\lambda) A(a, \lambda) B(b', \lambda) \left(1 \pm A(a', \lambda) B(b, \lambda) \right) d\lambda \qquad (2.68)$$

where the $\pm$ accounts for different grouping of the added quantity. If we now apply the triangle inequality and use the fact that $|A(a, \lambda)|, |B(b, \lambda)| \leq 1$ and $1 \pm A(a', \lambda)B(b', \lambda) \geq 0$ we can write:

$$|P(a, b) - P(a, b')| \leq \int \rho(\lambda)(1 \pm A(a', \lambda)B(b', \lambda)) d\lambda \qquad (2.69)$$

$$+ \int \rho(\lambda)(1 \pm A(a', \lambda)B(b, \lambda)) d\lambda \qquad (2.70)$$

Finally, using $\int \rho(\lambda) d\lambda = 1$, we have:

$$|P(a, b) - P(a, b')| \leq 2 \pm [P(a', b') + P(a', b)] \qquad (2.71)$$

Which includes the CHSH inequality in the form:

$$S = P(a, b) - P(a, b') + P(a', b') + P(a', b)$$
$$-2 \leq S \leq 2 \qquad (2.72)$$

Since I_a and I_b can be an entire measurement system, we can think of it as a filter followed by a detector, which in fact is our experimental apparatus (see later chapters for details). In this case $A(a)$ and $B(b)$ would denote detection or non-detection of the particle and we can think of applying the inequality directly to the experimental counting rates.

In order to derive an experimental prediction from (2.72) we need to make an additional assumption: the probability of joint detection of the two particles must be independent of the particular setting of a and b. Now, if the flux into each experimental apparatus is also a constant, then the rate of coincidence detection, $C(a, b)$, is proportional to $p_\pm(a, b)_\pm$, which is the probability to have $A(a) = \pm 1$ and $B(b) = \pm 1$. If this is the case, we can write the expectation value $P(a, b)$ as follows:

$$P(a, b) = E(a, b) = p_{++}(a, b) + p_{--}(a, b) - p_{+-}(a, b) - p_{-+}(a, b) \quad (2.73)$$

Where, e.g., $p_{++}(a, b)$ is the probability of obtaining $+1$ along a and $+1$ along b. From now on will call $P(a, b) = E(a, b)$ since this number can be negative and therefore is not a classical probability. It follows from the previous assumptions a useful expression for the $E(a, b)$:

$$E(a, b) = \frac{C_{++}(a, b) + C_{--}(a, b) - C_{+-}(a, b) - C_{-+}(a, b)}{C_{++}(a, b) + C_{--}(a, b) + C_{+-}(a, b) + C_{-+}(a, b)} \qquad (2.74)$$

2.6 Single Qubit Tomography

In this section we address the problem of reconstructing the density matrix of an identical ensemble of a given quantum state. This problem is known as quantum state tomography[28, 29, 30]. We will focus on the measurement of a single qubit since it is most relevant to our work and refer to the bibliography for further information.

We already demonstrated, Eq. 2.15 how it is possible to write the general density matrix of a qubit in terms of the Pauli matrix:

$$\rho = \frac{1}{2} \sum_{i=0}^{3} S_i \sigma_i \tag{2.75}$$

where the σ_i are just the Pauli matrix. The S parameters instead are defined as follows:

$$S_i = Tr\left\{\sigma_i \rho\right\} \tag{2.76}$$

The S parameter is therefore just the expectation value of the state ρ on the observable σ (this is equivalent to the claim that the four σ_i form a complete basis for the Hilbert space of the single qubit). For any pure state $\sum_{i=0}^{3} S_i = 1$ and ,as a necessary consequence for normalization, $S_0 = 1$. Each of these parameters corresponds to a specific pair of projective measurement:

$$
\begin{aligned}
S_0 &= P_{|0\rangle} + P_{|1\rangle} \\
S_1 &= P_{\frac{1}{\sqrt{2}}(|0\rangle+|1\rangle)} - P_{\frac{1}{\sqrt{2}}|1\rangle-|1\rangle} \\
S_2 &= P_{\frac{1}{\sqrt{2}}(|0\rangle+i|1\rangle)} - P_{\frac{1}{\sqrt{2}}(|1\rangle-|1\rangle)} \\
S_0 &= P_{|0\rangle} - P_{|1\rangle}
\end{aligned}
\tag{2.77}
$$

where P_ϕ is the probability to measure the state $|\phi\rangle$. Since $P_{|\phi\rangle} + P_{|\phi^\perp\rangle} = 1$, we an write:

$$
\begin{aligned}
S_0 &= 1 \\
S_1 &= 2P_{\frac{1}{\sqrt{2}}(|0\rangle+|1\rangle)} - 1 \\
S_2 &= 2P_{\frac{1}{\sqrt{2}}(|0\rangle+i|1\rangle)} - 1 \\
S_0 &= 2P_{|0\rangle} - 1
\end{aligned}
\tag{2.78}
$$

If we can measure the S_i parameters experimentally, we can now reconstruct the density matrix. We must therefore implement an arbitrary projective measurement stage and this is completely described in section 3.6.

Chapter 3

Silicon Photonics

3.1 The Silicon on Insulator Platform

Silicon photonics is the recent but rapidly growing field where silicon is used as an optic medium[31, 32]. A standard semiconductor in electronic industry, silicon is a well known material with complete compatibility with CMOS and telecommunication technology. The use of telecommunication wavelengths ($\approx 1.55\mu m$) has the advantage of allowing access to the developments of classical photonics, such as very low loss optical fibres. In particular, the Silicon on Insulator platform (SoI), where the silicon layer of interest lies on top (and eventually is surrounded by) a layer of SiO_2, is particularly interesting as it enables the implementation of very compact single mode waveguides ($0.45 - 0.5\mu m$) . This feature greatly enhances the degree of complexity of integrated circuits, which are a current research topic.

In this section we first give a basic introduction of the classical and quantum behaviour of the most important elements which build up our circuit: single mode waveguides, MMI couplers, single photon sources and Mach-Zehnder interferometers as a tomography stage. The design of the chip was based upon previous studies and was not part of this thesis. Nevertheless, we will give a rather detailed description of the criteria used to define the different structures in the circuit, together with the design specification of each building block.

3.2 Waveguides

The waveguides were designed to be single mode for TE input fields at 1550 nm. We use term single mode rather loosely here, since the waveguide profile allows a single TM mode as well. This can be justified because the two modes

are orthogonal and remain orthogonal even when bends are present. Note that this is the case only if there is one possible TE mode, otherwise bends would introduce crosstalk with random probabilities and phase, making the system no longer suitable for single photon routing.
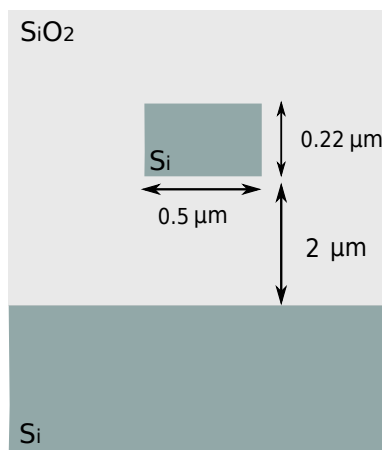

Figure 3.1: Cross section of a SoI waveguide

3.3 Multimode Interference Coupler

In this experiment MMIs were designed to be 2.8 μm x 27 μm in order to equally split bright light into two different paths and to witness quantum interference. We shall now describe the underlying physical principle, although in the rest of the thesis we will always consider it a "black box" with a scattering matrix akin to the balanced beam splitter one. As a result, we will thus be able to extend the results of chapter 1 to an MMI coupler.In the remaining of the section, we will follow the treatment given in [33].
In general, an MMI is composed of three distinctive zones: a central uniform slab, which is usually designed to support more than three modes, and an arbitrary number of input and output waveguides, which are usually single mode. An MMI with N input waveguides and M output ones, is usually referred to as a NxM MMI coupler. The multimode waveguide we consider is, as apparent from Fig. 3.2, a step index one, with the dimension on the x-axis far smaller than the other two that can be normally considered single mode, therefore reducing the dimensionality of the problem. As a result, it is justified to assume that the modes have the same transverse behaviour
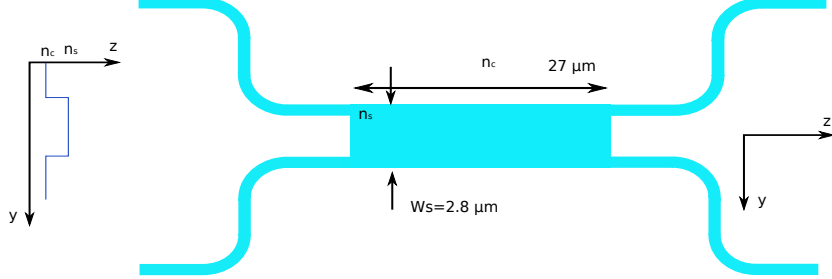
everywhere in the waveguide.

Figure 3.2: Schematic of an MMI coupler

As the figure shows, we have a waveguide with refractive index n_s and width W_s which supports m later mode labelled as $\nu = 0, 1 \cdots (m-1)$ at an arbitrary free space wavelength λ_0. If we call the lateral wavenumber $k_{y\nu}$ and β_ν the propagation constant, we can write the dispersion relation as follows:

$$k_{y\nu}^2 + \beta_\nu^2 = k_0^2 n_s^2 \tag{3.1}$$

where $k_0 = \frac{2\pi}{\lambda_0}$ and $k_{y\nu} = \frac{(\nu+1)\pi}{W_{e\nu}}$. In the expression for the lateral wavenumber W_m is substituted by the effective width $W_{e\nu}$ which takes into account the lateral penetration of the mode into the lower index medium. This effective length is associated with the Goos-Hänchen shift and can be evaluated, if one approximates $W_{e\nu}$ with W_{e0} of the fundamental mode, as follows:

$$\begin{aligned} W_{e\nu} \simeq W_e = W_s + \left(\frac{\lambda_0}{\pi}\right)\left(\frac{n_c}{n_s}\right)^{2\sigma}\left(n_s^2 - n_c^2\right)^{-\frac{1}{2}} \\ = W_s + \gamma \end{aligned} \tag{3.2}$$

where n_c is the cladding refractive index and $\sigma = 0$ for TE and $\sigma = 1$ for TM. If we evaluate the penetration depth (which is just the second part of RHS of (3.2)) in our system we find that $\gamma = 156\, nm$. This is the 5.5% of the MMI coupler width.
From (3.1) we can now evaluate the propagation constant β_ν :

$$\beta_\nu = \sqrt{k_0^2 n_s^2 - k_{y\nu}^2} = k_0 n_s \sqrt{1 - \frac{k_{y\nu}^2}{k_0^2 n_s^2}} \tag{3.3}$$

Now, since $k_{y\nu}^2 \ll k_0^2 n_s^2$ we can use the binomial expansion and stop at the first order to get:

$$\beta_\nu \simeq k_0 n_s - \frac{(\nu + 1)^2 \pi \lambda_0}{4W_{e\nu}^2 n_s} \tag{3.4}$$

With the help of the last equation we can now define a key parameter of the MMI which, as we will show soon after, will help us to give a first order estimation of the MMI length when working as a 2x2 beam splitter. We define the beat length of the two lowest order modes as:

$$L_\pi = \frac{\pi}{\beta_0 - \beta_1} \simeq \frac{4n_s W_{e\nu}^2}{3\lambda_0} \tag{3.5}$$

and express the propagation constants spacing as:

$$(\beta_0 - \beta_\nu) = \frac{\nu (\nu + 2) \pi}{3L_\pi} \tag{3.6}$$

We now turn our attention to a Guided-Mode Propagation Analysis. We consider an input field $\Psi (y, 0)$ at $z = 0$ (obviously totally contained in W_e) . We want to decompose the input field as a sum of all the modal field inside the multimode waveguide:

$$\Psi (y, 0) = \sum_\nu c_\nu \psi_\nu (y) \tag{3.7}$$

where the summation should in principle include radiative as well as guides modes. The coefficients of the expansion can be expressed in terms of overlap integrals:

$$c_\nu = \frac{\int \Psi (y, 0) \psi_\nu (y) \, dy}{\sqrt{\int \psi_\nu^2 (y) \, dy}} \tag{3.8}$$

If the spatial spectrum of the input field is narrow enough to excite only guided modes we can write:

$$\Psi (y, 0) = \sum_{\nu=0}^{m-1} c_\nu \psi_\nu (y) \tag{3.9}$$

At a generic distance z, the field will now be a superposition of all the guided mode field distribution:

$$\Psi (y, z) = \sum_{\nu=0}^{m-1} c_\nu \psi_\nu (y) \exp \left[i \left(\omega t - \beta_\nu z \right) \right] \tag{3.10}$$

We now take out of the sum the phase of the fundamental mode, we drop it, and assuming the time dependence of the exponential implicit from here on we get:

$$\Psi\left(y,z\right) = \sum_{\nu=0}^{m-1} c_\nu \psi_\nu\left(y\right) \exp\left[i\left(\beta_0 - \beta_\nu\right)z\right] \tag{3.11}$$

Finally, if we evaluate the last expression fro $z = L$ and substitute (3.6) we find:

$$\Psi\left(y,L\right) = \sum_{\nu=0}^{m-1} c_\nu \psi_\nu\left(y\right) \exp\left[i\frac{\nu\left(\nu+2\right)\pi}{3L_\pi}L\right] \tag{3.12}$$

We can now easily see how, under certain circumstances, the field $\Psi\left(y,L\right)$ will be a reproduction, in single or multiple images, of the input field. This effect is called *self-imaging* and is a property of multimode waveguides. We can for example see that (3.12) will be an exact replica of the input field if two conditions are satisfied. The first case is when:

$$\exp\left[i\frac{\nu\left(\nu+2\right)\pi}{3L_\pi}L\right] = 1 \tag{3.13}$$

In this case all the excited modes will interfere with same relative phase of $z = 0$ and the image will be a direct replica of $\Psi\left(y,0\right)$. The second condition is less obvious and is fulfilled when:

$$\exp\left[i\frac{\nu\left(\nu+2\right)\pi}{3L_\pi}L\right] = \left(-1\right)^\nu \tag{3.14}$$

In this case the replica will be a mirrored image with respect to the z-axis. This is a consequence of the symmetry of the structure we are considering with respect to the plane $y = 0$, which as a result implies:

$$\psi_\nu\left(-y\right) = \begin{cases} \psi_\nu\left(y\right), & \text{for } \nu \text{ even} \\ -\psi_\nu\left(y\right) & \text{for } \nu \text{ odd} \end{cases} \tag{3.15}$$

Both conditions are satisfied when :

$$L = p\left(3L_\pi\right) \quad \text{with} \quad p = 0,1,2\ldots \tag{3.16}$$

Here, we considered p as an integer. This way, p denotes the nature of the single replica, direct or mirrored, and can be used to design bar and cross couplers. Furthermore we are indeed interested in design a beam splitter and we must therefore consider the formation of multiple images. This is easily

done by considering the images obtained half way between direct and mirror image positions, i.e. at distances:

$$L = \frac{p}{2}\left(3L_\pi\right) \quad \text{with} \quad p = 1, 3, 5 \ldots \tag{3.17}$$

If we evaluate the total field at these distances:

$$\Psi\left(y, \frac{p}{2}3L_\pi\right) = \sum_{\nu=0}^{m-1} c_\nu \psi_\nu\left(y\right) \exp\left[i\nu\left(\nu+2\right)p\left(\frac{\pi}{2}\right)\right] \tag{3.18}$$

If we now make use of the fact that the factor $\nu\left(\nu+2\right)$ is even for ν even and odd for ν odd, together with symmetric properties of the field we considered before, The output field can be written as:

$$\begin{aligned}
\Psi\left(y, \frac{p}{2}3L_\pi\right) &= \sum_{\nu even} c_\nu \psi_\nu + \sum_{\nu odd} \left(-i\right)^p c_\nu \psi_\nu \\
&= \frac{1+\left(-i\right)^p}{2}\Psi\left(y, 0\right) + \frac{1-\left(-i\right)^p}{2}\Psi\left(-y, 0\right)
\end{aligned} \tag{3.19}$$

The last equation shows clearly that the output field is a pair of images, in quadrature and with amplitudes $\frac{1}{\sqrt{2}}$, of the input field. We can now give a first estimation of the length of the MMI when it must work as a 3-dB coupler. In fact, if we set $p = 1$:

$$L = \frac{3}{2}L_\pi = \frac{2n_s W_{e\nu}^2}{\lambda_0} \approx 39\mu m \tag{3.20}$$

Where we consider $\lambda = 1.55\ \mu m$. This number significantly differs from our design and should be regarded only as a first order approximation. This is a consequence of the fact that we are using only the first two mode to estimate L_π, while the real device has more than two modes.

3.4   Diffraction Gratings

3.4.1   1-Dimensional

High refractive index contrast allows drastic reduction of the size of the optical circuits, making the SoI platform a very promising candidate for the production of large scale integrated optical circuits[34, 35, 36]. However, interfacing a 10 μm diameter with a 500 nm waveguide becomes a serious challenge, due to the huge mismatch between the respective modes. This

problem can be solved with a range of different approach but in this experiment we used one dimensional grating couplers. Grating couplers are simple one-dimensional periodic structure etched on top of the silicon waveguide. This way light can be directly coupled from a single mode fibre to the grating, which can be anywhere on the chip, and diffracted directly into the waveguide. An additional adiabatic taper laterally then slowly converts the mode from roughly 10 μm to 500 nm.
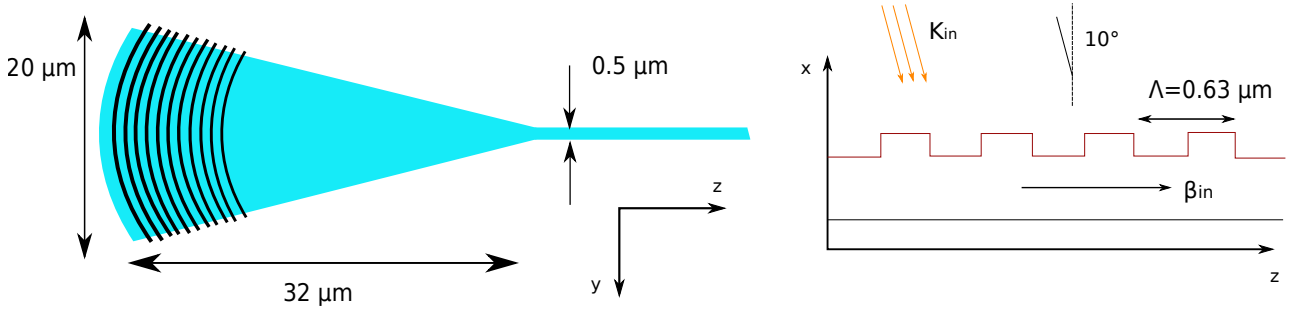

Figure 3.3: Geometry of a one dimensional grating coupler. The right image is section in the x-z plane.

We will now outline the operation principle of the device. The periodicity of the grating implies that the light will be diffracted in preferential directions. This can be understood if we assume the structure to be infinite and we analyse it from a bi-dimensional point of view, see Fig. 3.3. In this respect, the structure is just a Bragg diffraction grating and can be fully described by the relation:

$$k_{z,m} = \beta_{mode} + mK \tag{3.21}$$

where m is an integer and describes the m_{th} order of diffraction. $k_{z,m}$ is z projection of the wave vector of the diffracted wave.

As a consequence of the high index contrast at Si/SiO_2 interface, β_{mode} is not simply the mode wave vector, but one must consider an average between the propagation constant of the guided mode in the etched and unetched regions. We must therefore use an effective index $n_{eff}(\lambda)$ instead of n_{Si}. K is the reciprocal lattice vector and its module is $|K| = \frac{2\pi}{\Lambda}$. The Bragg condition directly determines the angle of diffraction since :

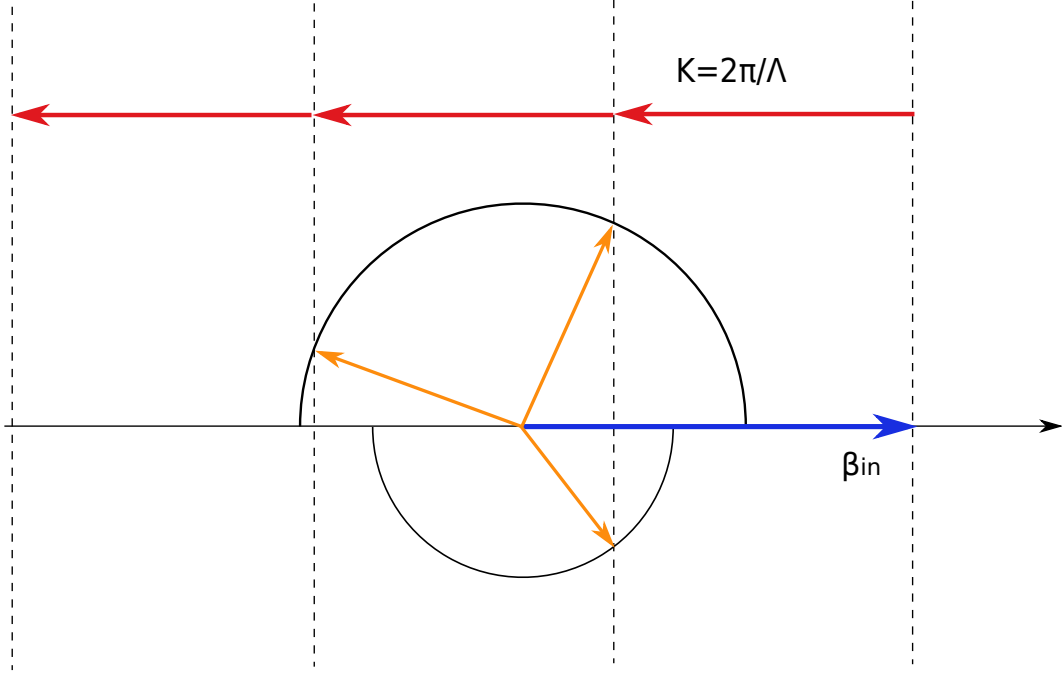$$k_{z,m} = \frac{2\pi n_{SiO_2} \sin(\theta_0)}{\lambda} \tag{3.22}$$

We can now write:

Figure 3.4: Graphical representation of the Bragg condition

$$\sin(\theta_0) = \frac{n_{eff}(\lambda)}{n_{SiO_2}} + m\frac{\lambda}{n_{SiO_2}\Lambda} \tag{3.23}$$

Simulations can give us an estimation of the effective index, which is found to be $n_{eff}(\lambda) = 2.6963$. Moreover, we constraint θ_0 to be $10°$ so that we can now calculate the pitch $\Lambda = 634.1\ nm$ (where we set $m = -1$). This is already a very accurate approximation of the correct grating pitch and can be further improve with numerical simulations. One might be puzzled by our choice of the diffraction angle, as the vertical coupling might appear to be the most natural solution. Let us consider then of perfect vertical coupling to the chip:

$$\beta_{mode} = K \tag{3.24}$$

with $m = -1$. Although this condition produces a first order diffraction directly into the superstrate, a second order diffraction also occurs back into the waveguide:

$$k_{z,-2} = \beta_{mode} - 2K = -\beta_{mode} \tag{3.25}$$

This second order of diffraction is highly unwanted and can drastically

reduce the coupling efficiency of the grating, thus we opted for a detuned configuration.

A last expedient was used in order to reduce the area of the device. In fact, if a rectangular coupler would require only 10 μm x 10 μm, a very long taper would still be needed (around 150 μm) to match the different size of the modes, as already explained. This can be avoided by using a curved grating lines instead of straight ones. Light coming from the fibre will now not only be coupled to the waveguide plane but also focused directly onto the waveguide aperture. It can be shown that a focusing grating can be obtained by curving the grating lines according to:

$$q\lambda = n_{eff}\sqrt{y^2 + z^2} - zn\cos\left(\theta_c\right) \qquad (3.26)$$

where θ_c is the angle between the fibre and the chip and q is a different integer number for each line. This way the grating effective footprint can be scaled down by a factor of eight without any drop in the performance.

3.4.2 2-Dimensional

A key component of our experiment, as we will explain in greater details in the following chapter, is the 2D grating coupler[37]. As we can see from Fig 3.5 this is just a square photonic crystal structure, invariant for 90° rotations. The theory of this device, which can work either as a output or input coupler, is readily explained in terms of a superposition of 1D grating couplers. In fact, a 2D grating is just a square array of holes which satisfy the Bragg condition in two perpendicular directions. In this fashion light with different polarization is coupled to two nearly orthogonal waveguides. The TM component will also be rotated to TE and the grating will incorporate the functionality of a coupler, a polarization beam splitter and a rotator for the TM component. The ratio of the incoming light coupled to each fibre will be therefore polarization dependent, but the total coupling efficiency considering both waveguides will not (aside for some polarization dependent losses, which are negligible for this experiment).

We now have two different problems to solve in order to increase the efficiency of the structure. Firstly, the access waveguides have to be tilted inwards. This can be understood by rewriting the Bragg condition as follows:

$$k_{z,i} = k_{in,proj} + K_i \tag{3.27}$$

where $i = 1, 2$ and $K_1 = \frac{2\pi}{\Lambda}\vec{i}$, $K_2 = \frac{2\pi}{\Lambda}\vec{j}$. Also:

$$k_{in,proj} = \frac{2\pi n}{\Lambda} \sin(\theta_0) \left(\frac{1}{\sqrt{2}}\vec{i} + \frac{1}{\sqrt{2}}\vec{j} \right) \tag{3.28}$$

so that $k_{z,1}$ and $k_{z,2}$ are no longer orthogonal as it is apparent from the image. The access waveguides must therefore be tilted in order not to reduce the coupling efficiency (for 10° fibre a 3° tilt was applied).

In the quantum regime, this device can be used to coherently couple a quantum state from the "path" basis, usually utilized in integrated circuits, to the polarization basis, which is the most natural for transmitting quantum information through a fibre. The fidelity of this "Path to Polarization" converter (PPC) has been analysed thoroughly and the experimental results obtained are in the relative section.

10 µm

d=0.39 µm

10 µm

Λ=0.63 µm
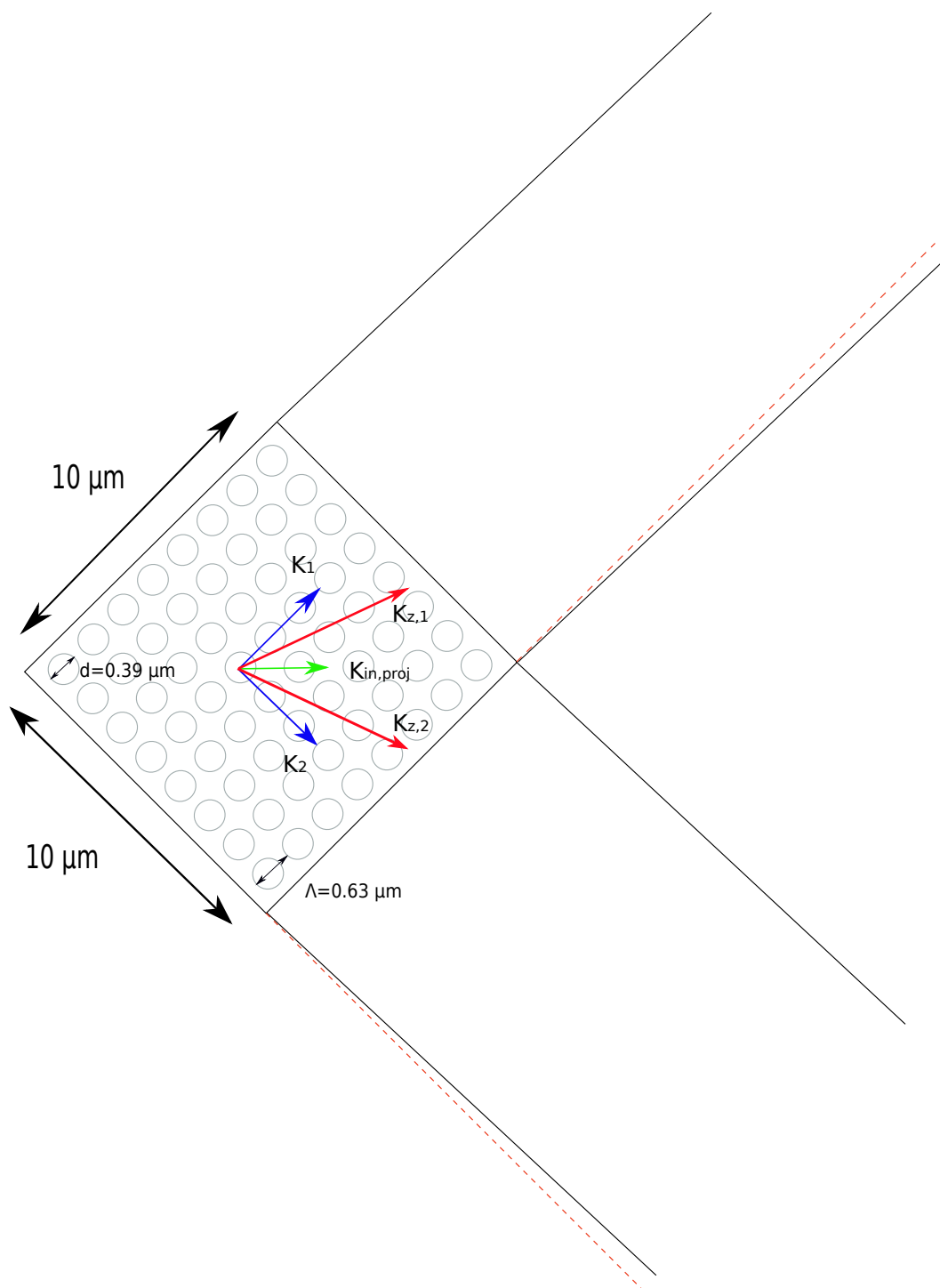
K_1

$K_{z,1}$

$K_{in,proj}$

$K_{z,2}$

K_2

Figure 3.5: Geometry of a two dimensional grating coupler. The two waveguides are slightly tilted in order to accommodate for the new phase matching condition.

3.5 Integrated Single Photon Sources

In this section we will describe in some details the integrated single photon sources we used, which were based on a previous study [13] and refer to the Bibliography for further information. Before going into details we give some general remarks about the χ_3 effect in silicon, which is the underlying physical process we use to generate correlated single photons.

3.5.1 Pair Generation in Silicon

Spontaneous four wave mixing is third order non linear effect whereby, in the non-degenerate case we are interested, two photons of the pump are annihilated in order to generate two photons, the signal and the idler, at different wavelengths. Since the strength of χ_3 processes is dependent on the refractive index[19] of the material like $\chi_3 \propto (1-n)^4$, a rather strong interaction is expected ($n_{Si} = 3.48$). In literature the strength of the non linearity is usually expressed in terms of $n_2 = \frac{3}{2n_0^2 \epsilon_0 c} \chi^{(3)}$, where n_2 is the self focusing index effect $n = n_0 + n_2 I$. For silicon the value oscillates between $n_2 = 4 - 9 \times 10^{-14} \, cm^2 \, W^{-1}$. In SoI platform the high index contrast requires the waveguide core to be between 450 and 550 nm (for a thickness of 220 nm) and translates in an effective non-linear coupling constant far higher than in bulk silicon. Typical values are $\gamma \approx 460 \, m^{-1} W^{-1}$ at communication wavelength.
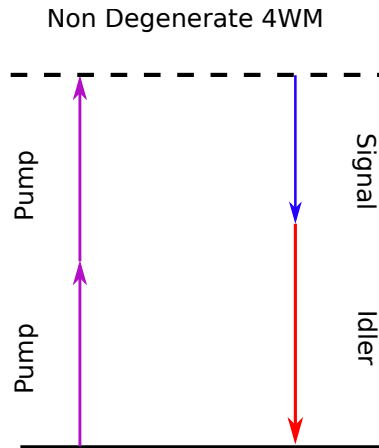

Figure 3.6: Energy diagram for non degenerate SFWM

The hamiltonian is composed of two parts:

$$H = H_L + H_{NL} \tag{3.29}$$

where

$$H_L = \int dk \hbar \omega_k a_k^\dagger a_k$$

$$H_{NL} = -\gamma_0 \int dk_1 dk_2 dk_3 dk_4 \hbar \omega_k a_{k_1}^\dagger a_{k_2}^\dagger a_{k_3} a_{k_4} \exp\left[i(k_4 + k_3 - k_2 - k_1)z\right] + h.c.$$

where γ_0 is the effective non linear coupling constant. It can be shown[38, 39] that, starting with a coherent state $|\alpha\rangle$, the output state in a straight waveguide with the defined hamiltonian is, to first order:

$$|\psi_{out}\rangle = \left[1 + \frac{\gamma_0 \alpha^2 L}{\sqrt{2}} \int dk_1 dk_2 \Phi(k_1, k_2) a_{k_1}^\dagger a_{k_2}^\dagger \right] |\alpha\rangle \otimes |vac\rangle \tag{3.30}$$

with L the waveguide length and Φ is the joint spectral intensity of the biphoton state. We will use this result in the next section, without demonstration, in order to calculate the output state of our sources.

3.5.2 Theory of Operation

Before going into some technical details we give a qualitative description of the state generation. In our device we have two photon pair sources, each of which is composed by a spiralled waveguide $2\,cm$ long. The bright pump from an off-chip laser is equally split by a balanced MMI and both sources are pumped simultaneously. In this region, the $\chi^{(3)}$ spontaneous four wave mixing non-degenerate pairs of photons, called signal and idler, are created by annihilating two photons of the pump. By operating in the weak pump regime, only one pair is likely to generated, and the sources yield the path entangled NOON state:

$$|\psi\rangle = \frac{|2\rangle_t |0\rangle_b - |0\rangle_t |2\rangle_b}{\sqrt{2}} \tag{3.31}$$

A thermal phase shifter on one source only allows the dynamical control of the relative phase:

$$|\psi\rangle = \frac{|2\rangle_t |0\rangle_b - e^{2\theta i} |0\rangle_t |2\rangle_b}{\sqrt{2}} \tag{3.32}$$
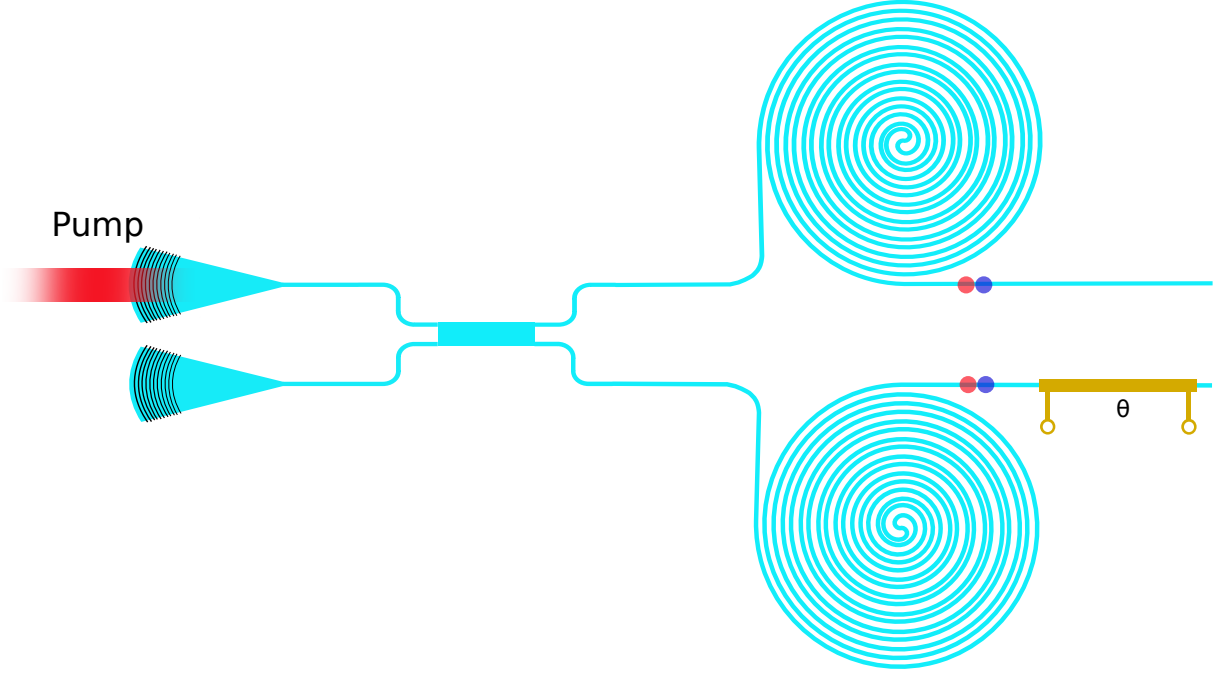
Figure 3.7: Integrated single photon source.

where the phase applied to the single photons is doubled when compared to the bright pump. We now give a demonstration of how the NOON state is obtained, starting from the hamiltonian (3.30) of the SFWM processes for a straight waveguide with $\chi^{(3)}$ non linearity.

We assume the pump to be monochromatic (ω_p, k_p) and we call the filter response with which we post select signal and idler (off-chip) $f_s(k_s)$ and $f_i(k_i) = f_i(2k_p - k_s)$. Thus:

$$|\psi_{out}\rangle = \left[1 + \frac{\gamma_0 \alpha^2 L}{\sqrt{2}} \int dk_i dk_s f_s(k_s) f_i(2k_p - k_s) sinc\left(\frac{\Delta k L}{2}\right) a_{k_s}^\dagger a_{2k_p - k_s}^\dagger \right] |\alpha\rangle \otimes |vac\rangle$$

where

$$\Delta k = 2k_p - k_s - k_i$$

We want to rewrite the output state with a lighter notation:

$$|\psi_{out}\rangle = \left[1 + \gamma_{eff} \alpha^2 A_{i,s}^\dagger \right] |\alpha\rangle \otimes |vac\rangle \qquad (3.33)$$

where γ_{eff} is the effective pair generation coefficient and $A_{i,s}^\dagger$ is the generation operator for signal and idler. The phase matching bandwidth is

governed by the *sinc*() function, although in practice the narrow band filters only select a very small and flat part of the *sinc*() itself. In this regime the output state is proportional to L^2, where L is the length of the spiral.

We can now demonstrate how the path entangled NOON state is generated, starting from a coherent state which, after the first beam splitter, becomes:

$$|\alpha\rangle \rightarrow |\sqrt{\eta}\alpha\rangle \left| i\sqrt{1-\eta}\alpha \right\rangle \tag{3.34}$$

We now have pair generation in both sources:

$$|\sqrt{\eta}\alpha\rangle \left| i\sqrt{1-\eta}\alpha \right\rangle \rightarrow \left[1 + \frac{\gamma_0\alpha^2 L}{\sqrt{2}} \int dk_1 dk_2 \Phi(k_1, k_2) c_{k_1}^\dagger c_{k_2}^\dagger \right] |\alpha\rangle$$

$$\left[1 + \frac{\gamma_0\alpha^2 L}{\sqrt{2}} \int dk_1 dk_2 \Phi(k_1, k_2) d_{k_1}^\dagger d_{k_2}^\dagger \right] \left| i\sqrt{1-\eta}\alpha \right\rangle |vac\rangle$$

We now neglect the second order term $\propto \gamma_0^2$ since this is negligible when compared to the probability of generating one pair. Therefore:

$$|\psi_{out}\rangle = 1 + \frac{\gamma\alpha^2 L}{\sqrt{2}} \int dk_1 dk_2 \Phi(k_1, k_2) \left[\eta c_{k_1}^\dagger c_{k_2}^\dagger - (1-\eta) d_{k_1}^\dagger d_{k_2}^\dagger \right] \left| i\sqrt{1-\eta}\,\alpha \right\rangle |\sqrt{\eta}\,\alpha\rangle |vac\rangle$$

and after the phase shifter (on the d mode only):

$$|\psi_{out}\rangle = 1 + \frac{\gamma\alpha^2 L}{\sqrt{2}} \int dk_1 dk_2 \Phi(k_1, k_2) \left[\eta c_{k_1}^\dagger c_{k_2}^\dagger - e^{2\theta i}(1-\eta) d_{k_1}^\dagger d_{k_2}^\dagger \right] \left| i\sqrt{1-\eta}\,\alpha \right\rangle |\sqrt{\eta}\,\alpha\rangle |vac\rangle$$

If we then post select the two single photons (which we relabel $1, 2 \rightarrow s, i$) and get rid of the pump mode (and assuming $\eta = \frac{1}{2}$):

$$|\psi_{out}\rangle = \frac{\gamma\alpha^2 L}{2\sqrt{2}} \int dk_1 dk_2 \Phi(k_1, k_2) f_s(k_s) f_i(2k_{\omega_p} - k_s) \left[|1_s\rangle_t |1_i\rangle_t |0_s\rangle_b |0_i\rangle_b - e^{2\theta i} |0_s\rangle_t |0_i\rangle_t |1_s\rangle_b |1_i\rangle_b \right]$$

where $f_s(k_s)$ and $f_i(k_i)$ are the transfer function of the filter used in the post selection process. As we already mentioned, in practice the spectral integral almost entirely depends on the bandwidth of the filters (usually 1 *nm*). For the rest of this thesis we will forget the spectral distribution of the photons and consider only one wavelength (that is we will go back to a discrete variable treatment). This is justified as long as we are in a flat zone of the phase matching condition and the filters only select a small portion of it, as it always the case in our experiments.

3.6   Single Qubit Projective Measurement Stage

In order to implement an arbitrary projective measurement stage, a Mach-Zehnder interferometer with an additional phase shifter on one input is used[40, 41]. The phase control is implemented by two thermal phase shifter, which take advantage of the thermo-optic coefficient of silicon. In literature this coefficient is estimated to be around $\frac{dn}{dT} \simeq 1 \times 10^{-5} K^{-1}$. The balanced beam splitters are implemented by MMI couplers with same design described in the relative section. The resistive heaters were made by a Ti/TiN metal layer and were designed to be 50 μm long. The heaters were then connected to the PCB with a wire-bonding technology.
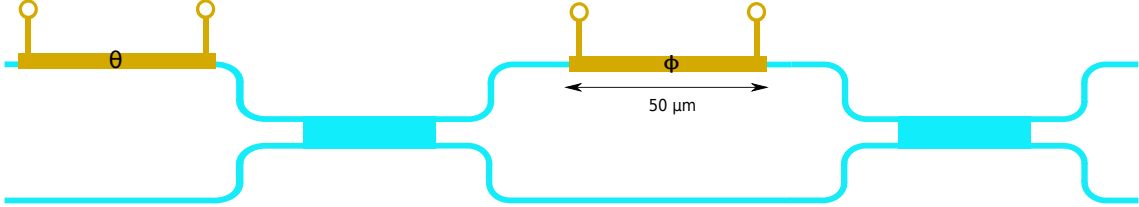
Figure 3.8: Schematic of a Measurement stage, which consists of Mach-Zehnder interferometer with an additional phase shifter.

The tomography stage characterisation will be detailed in the experimental section. From here on we will refer to this stage as $A(\theta, \phi)$ (or as $B(\theta, \phi)$ for Bob's one). We want to show how it is possible to decompose the action of this stage in terms of the Pauli matrices and the Hadamard gate, so that we can prove what is the action of the state on a generic qubit. From the definition of $R_x(\theta)$ together with the expansion (2.1), we can easily write:

$$R_x(\theta) = \exp\left(-i\theta\frac{X}{2}\right) = R_z(-\frac{\pi}{2}) \cdot R_y(\theta) \cdot R_z(\frac{\pi}{2}) \qquad (3.35)$$

But for $\theta = -\frac{\pi}{2}$, we simply have the matrix of a balanced beam splitter:

$$R_x(-\frac{\pi}{2}) = R_z(-\frac{\pi}{2}) \cdot R_y(-\frac{\pi}{2}) \cdot R_z(\frac{\pi}{2}) \qquad (3.36)$$

We can write this in terms of an Hadamard gate if we notice that:

$$H = -i\, R_z(-\pi)R_y(-\frac{\pi}{2}) \qquad (3.37)$$

Then:

$$UBS = i\, R_z(\frac{\pi}{2}) \cdot H \cdot R_z(\frac{\pi}{2}) \tag{3.38}$$

The Unitary matrix of the Mach-Zehnder is now easily found:

$$U_{MZI} = BSe^{i\phi Z}BS \tag{3.39}$$

and if we add the phase shifter and write all terms explicitly:

$$A\left(\theta,\phi\right) = -e^{i\frac{\theta}{2}Z}e^{-i\frac{\pi}{4}Z}He^{-i\frac{\pi}{4}Z}e^{i\frac{\phi}{2}Z}e^{-i\frac{\pi}{4}Z}He^{-i\frac{\pi}{4}Z} \tag{3.40}$$

We can write the last expression in a simpler form with the aid of:

$$U_{MZI} = e^{i\frac{\phi}{2}Y} \cdot X \tag{3.41}$$

which can be verified by straightforward application of the previous definitions. Then:

$$A\left(\theta,\phi\right) = e^{i\frac{\phi}{2}Y} \cdot X \cdot e^{i\frac{\theta}{2}Z} = e^{i\frac{\phi}{2}Y} \cdot e^{-i\frac{\theta}{2}Z} \cdot X \tag{3.42}$$

This unitary matrix allows arbitrary projective measurement from the computational basis. In order to prove this, let us consider an arbitrary state preparation starting from the computational basis, e.g. $|0\rangle$. The transformation is the temporal inverse of the projective measurement, that is:

$$A^\dagger\left(\theta,\phi\right) = X \cdot e^{i\frac{\theta}{2}Z} \cdot e^{-i\frac{\phi}{2}Y} \tag{3.43}$$

If we apply this transformation to $|0\rangle$:

$$\begin{aligned} A^\dagger\left(\theta,\phi\right)|0\rangle &= e^{-\frac{i\theta}{2}}\sin\left(\frac{\phi}{2}\right)|0\rangle + e^{\frac{i\theta}{2}}\cos\left(\frac{\phi}{2}\right)|1\rangle \\ &= \sin\left(\frac{\phi}{2}\right)|0\rangle + e^{i\theta}\cos\left(\frac{\phi}{2}\right)|1\rangle \end{aligned} \tag{3.44}$$

Where in the last equality we dropped a global phase factor. Aside from a change of reference for what concerns the ϕ angle, this is just the form of a generic qubit on the Bloch sphere. The direct transformation is therefore just a projection on the computational basis. Crucial to our experiment will be the possibility of setting the projective stage as an Hadamard gate. This can be easily implemented with the following choice of angles:

$$A\left(0,\frac{\pi}{2}\right) = \frac{1}{\sqrt{2}}\begin{pmatrix} 1 & 1 \\ 1 & -1 \end{pmatrix} \tag{3.45}$$

Chapter 4

Concept of the Experiment

In this chapter we give a full description of the circuit theory. We give a somewhat simplified treatment which does not take into account the dissipations inside the chip and full spectrum of the generated pairs (this last assumption is without loss of generality, since we can extend the results found for a single wavelength to the region of significant phase matching). Nevertheless, this analysis can give a clearer understanding of the physics underneath the experiment.

4.1   The Experiment in a Nutshell

Before going into the details we present the experiment with the intention of clarifying, in a non rigorous way, the various steps which comprise the full experiment.

Our goal is to demonstrate the possibility of generating, manipulating and ultimately distribute an entangled state between two chips, linked by a single mode fibre. We will refer to the first chip, where the entangled state is generated, as Alice's chip. The second chip will be Bob's chip, as it is traditional in EPR experiments.

The bright light pumped into the chip is equally split by the MMI to simultaneously pump both the spiral sources. As discussed before the state after the two sources and the thermal phase shifter is:

$$|\psi\rangle = \frac{|1_s 1_i\rangle_t |0_s 0_i\rangle_b - e^{(\theta_s + \theta_i)i} |0_s 0_i\rangle_t |1_s 1_i\rangle_b}{\sqrt{2}} \qquad (4.1)$$

where the subscripts s, i refer to the signal and idler photons while the t, b refer to the top and bottom source. Since the idler and signal photons are very close in wavelength ($\sim 5nm$, see next chapter for experimental details),

the phase shift applied is almost exactly the same and we can approximate $\theta_s \simeq \theta_i \simeq \theta$. Thus we can write:

$$|\psi\rangle = \frac{|2\rangle_t |0\rangle_b - e^{2\theta i} |0\rangle_t |2\rangle_b}{\sqrt{2}} \tag{4.2}$$
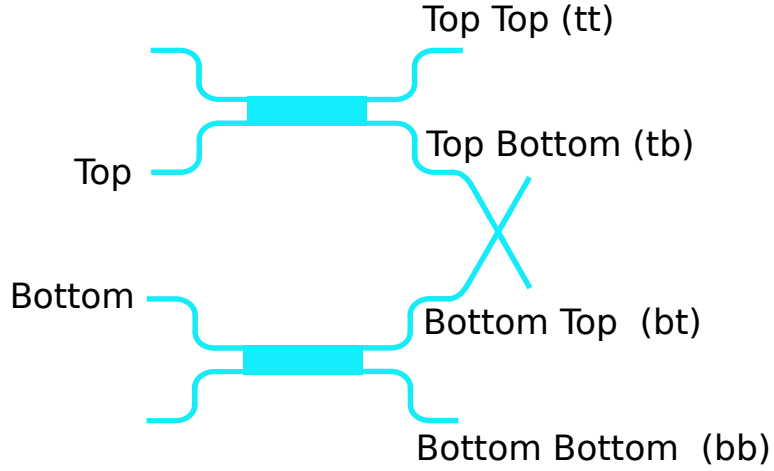
which is path entangled NOON state.

Figure 4.1: Labelling of the MMIs modes. (See also Fig. 4.2)

After the two MMI couplers and the cross, the state in the Fock basis is:

$$|\psi_{out}\rangle = \frac{1}{2\sqrt{2}} |1_s 0_i\rangle_{tt} |0_s 0_i\rangle_{tb} |0_s 1_i\rangle_{bt} |0_s 0_i\rangle_{bb} - e^{(2\theta i)} |0_s 0_i\rangle_{tt} |1_s 0_i\rangle_{tb} |0_s 0_i\rangle_{bt} |0_s 1_i\rangle_{bb}$$

where the modes are labelled after the Fig. 4.1. In the computational basis we can write this as:

$$|\psi_{out}\rangle = \frac{1}{\sqrt{2}} \Big(|0\rangle_{top} |0\rangle_{bottom} - e^{(2\theta i)} |1\rangle_{top} |1\rangle_{bottom} \Big) \tag{4.3}$$

When we set θ to be equal to $\frac{\pi}{2}$ or π we obtain two Bell's state :

$$|\Phi_\pm\rangle = \frac{1}{\sqrt{2}} \Big(|0\rangle_{top} |0\rangle_{bottom} \pm |1\rangle_{top} |1\rangle_{bottom} \Big) \tag{4.4}$$

The bottom qubit is now converted in a polarization entangled state, transmitted through a fibre to Bob's chip and reconverted into a path entangled state. The details of this conversion are explained in the experimental section. With the help of two arbitrary single qubit measurement stages we can now verify the violation of the Bell's inequality (in the CHSH form) and measure correlation fringes between the two chips.
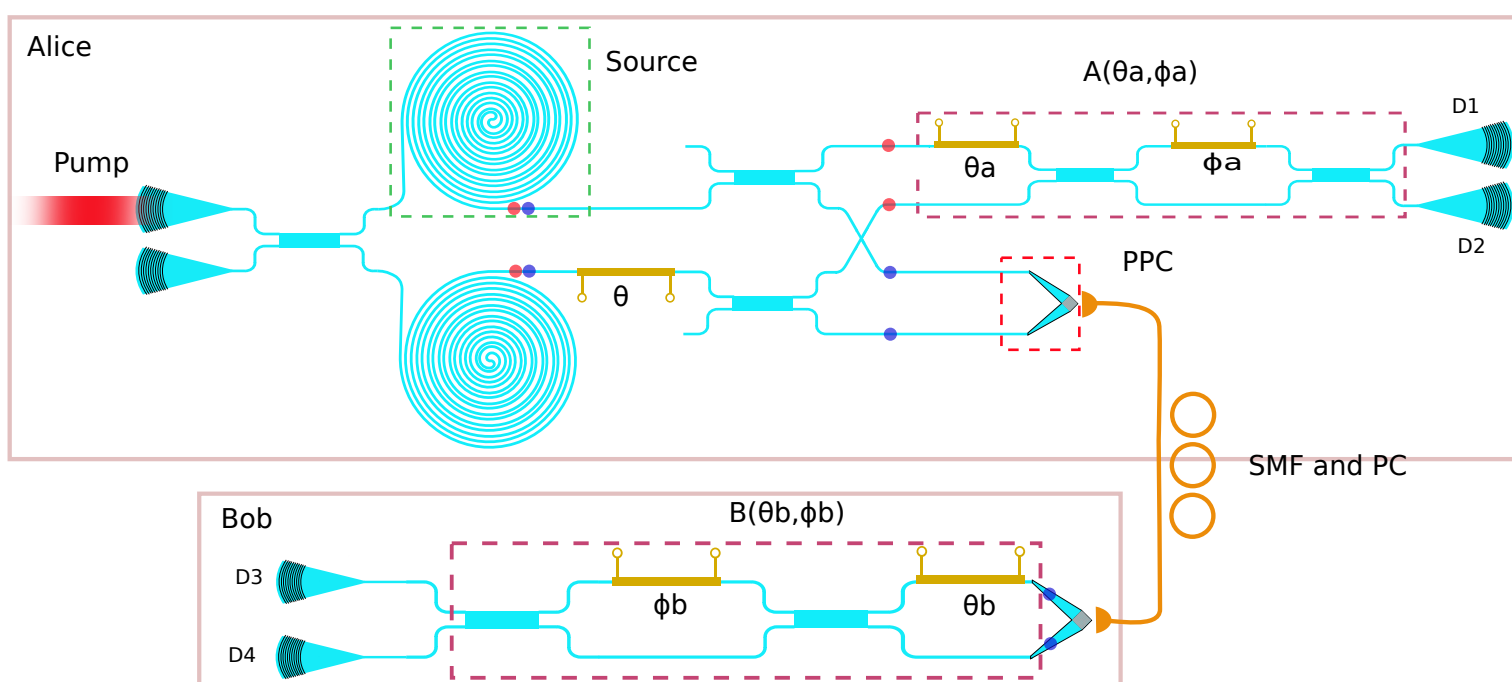
Figure 4.2: Alice's chip (top) and Bob's chip (bottom). The two chips are connected with $10\,m$ single mode fibre (SMF) with an additional polarisation controller (PC).

4.2 Full State Evolution

We now describe the state evolution starting from the state generated by the integrated sources. We must consider a total of eight modes, two different wavelengths and four spatial mode, which are labelled after the Fig. 4.1. By applying the beam splitter transformation, we obtain:

$$
\begin{aligned}
|\psi_{out}\rangle = U\,|\psi\rangle &= \frac{U}{\sqrt{2}}\left(a_{ts}^{\dagger}a_{ti}^{\dagger}\,|0_s0_i\rangle_t\,|0_s0_i\rangle_b - e^{(2\theta i)}\,|0_s0_i\rangle_t\,a_{bs}^{\dagger}a_{bi}^{\dagger}\,|0_s0_i\rangle_b\right)\\
&= \frac{1}{\sqrt{2}}\left(Ua_{ts}^{\dagger}U^{\dagger}Ua_{ti}^{\dagger}U^{\dagger}\,|0_s0_i\rangle_t\,|0_s0_i\rangle_b - e^{(2\theta i)}\,|0_s0_i\rangle_t\,Ua_{bs}^{\dagger}U^{\dagger}Ua_{bi}^{\dagger}U^{\dagger}\,|0_s0_i\rangle_b\right)\\
&= \frac{1}{2\sqrt{2}}\Big[\left(a_{tts}^{\dagger}+ia_{tbs}^{\dagger}\right)\left(ia_{tti}^{\dagger}+a_{tbi}^{\dagger}\right)|0_s0_i\rangle_{tt}\,|0_s0_i\rangle_{tb}\,|0_s0_i\rangle_{bt}\,|0_s0_i\rangle_{bb}\\
&\quad - e^{(2\theta i)}\,|0_s0_i\rangle_t\left(a_{bts}^{\dagger}+ia_{bbs}^{\dagger}\right)\left(ia_{bti}^{\dagger}+a_{bbi}^{\dagger}\right)|0_s0_i\rangle_{tt}\,|0_s0_i\rangle_{tb}\,|0_s0_i\rangle_{bt}\,|0_s0_i\rangle_{bb}\Big]
\end{aligned}
$$

The state after the MMIs and before the crossing is:

$$
\begin{aligned}
|\psi_{out}\rangle = \frac{1}{2\sqrt{2}}&i\,|1_s1_i\rangle_{tt}\,|0_s0_i\rangle_{tb}\,|0_s0_i\rangle_{bt}\,|0_s0_i\rangle_{bb} + |1_s0_i\rangle_{tt}\,|0_s1_i\rangle_{tb}\,|0_s0_i\rangle_{bt}\,|0_s0_i\rangle_{bb}\\
&- |0_s1_i\rangle_{tt}\,|1_s0_i\rangle_{tb}\,|0_s0_i\rangle_{bt}\,|0_s0_i\rangle_{bb} + i\,|0_s0_i\rangle_{tt}\,|1_s1_i\rangle_{tb}\,|0_s0_i\rangle_{bt}\,|0_s0_i\rangle_{bb}\\
&- e^{(2\theta i)}\Big[i\,|0_s0_i\rangle_{tt}\,|0_s0_i\rangle_{tb}\,|1_s1_i\rangle_{bt}\,|0_s0_i\rangle_{bb} + |0_s0_i\rangle_{tt}\,|0_s0_i\rangle_{tb}\,|1_s0_i\rangle_{bt}\,|0_s1_i\rangle_{bb}\\
&- |0_s0_i\rangle_{tt}\,|0_s0_i\rangle_{tb}\,|0_s1_i\rangle_{bt}\,|1_s0_i\rangle_{bb} + i\,|0_s0_i\rangle_{tt}\,|0_s0_i\rangle_{tb}\,|0_s0_i\rangle_{bt}\,|1_s1_i\rangle_{bb}\Big]
\end{aligned}
$$

The state after the intersection is found by formally substituting the index $tb \longrightarrow bt$ and vice versa. If we rearrange the terms for clarity, we finally get:

$$
\begin{aligned}
|\psi_{out}\rangle = \frac{1}{2\sqrt{2}}&\Big[i\,|1_s1_i\rangle_{tt}\,|0_s0_i\rangle_{tb}\,|0_s0_i\rangle_{bt}\,|0_s0_i\rangle_{bb} + |1_s0_i\rangle_{tt}\,|0_s0_i\rangle_{tb}\,|0_s1_i\rangle_{bt}\,|0_s0_i\rangle_{bb}\\
&- |0_s1_i\rangle_{tt}\,|0_s0_i\rangle_{tb}\,|1_s0_i\rangle_{bt}\,|0_s0_i\rangle_{bb} + i\,|0_s0_i\rangle_{tt}\,|0_s0_i\rangle_{tb}\,|1_s1_i\rangle_{bt}\,|0_s0_i\rangle_{bb}\Big]\\
&- e^{(2\theta i)}\Big[i\,|0_s0_i\rangle_{tt}\,|1_s1_i\rangle_{tb}\,|0_s0_i\rangle_{bt}\,|0_s0_i\rangle_{bb} + |0_s0_i\rangle_{tt}\,|1_s0_i\rangle_{tb}\,|0_s0_i\rangle_{bt}\,|0_s1_i\rangle_{bb}\\
&- |0_s0_i\rangle_{tt}\,|0_s1_i\rangle_{tb}\,|0_s0_i\rangle_{bt}\,|1_s0_i\rangle_{bb} + i\,|0_s0_i\rangle_{tt}\,|0_s0_i\rangle_{tb}\,|0_s0_i\rangle_{bt}\,|1_s1_i\rangle_{bb}\Big]
\end{aligned}
$$

This is the full state before the projective measurement stages. Depending on how we actually perform the measurement, we look at different parts of the full state. Our first aim is to test the quality of the entanglement produced on Alice's chip. In order to do this, we register the simultaneous detection of

signal and idler at port D1 and D2 respectively. The photons are post selected by means of an off-chip DWDM (see next chapter for information regarding the experimental setup). Since we are interested only in the coincidence detection, we can safely neglect all terms which have a photon in *bt* or *bb* waveguide:

$$|\psi_{out}\rangle = \frac{i}{\sqrt{2}} \Bigg[\Big(|1_s 1_i\rangle_{tt} |0_s 0_i\rangle_{tb} |0_s 0_i\rangle_{bt} |0_s 0_i\rangle_{bb} \Big)$$

$$- e^{(2\theta i)} \Big(|0_s 0_i\rangle_{tt} |1_s 1_i\rangle_{tb} |0_s 0_i\rangle_{bt} |0_s 0_i\rangle_{bb} \Big) \Bigg]$$

We now set the projective measurement stage $A(\theta, \phi)$ as an Hadamard gate by setting $\theta = 0$ and $\phi = \frac{\pi}{2}$. Therefore:

$$H |\psi_{out}\rangle = \frac{i}{2\sqrt{2}} \Bigg[\frac{(c_s^\dagger + d_s^\dagger)}{\sqrt{2}} \frac{(c_i^\dagger + d_i^\dagger)}{\sqrt{2}} - e^{(2\theta i)} \frac{(c_s^\dagger - d_s^\dagger)}{\sqrt{2}} \frac{(c_i^\dagger - d_i^\dagger)}{\sqrt{2}} \Bigg] |vac\rangle =$$

$$= \frac{i}{2\sqrt{2}} \Big[|1_s 1_i\rangle_{tt} |0_s 0_i\rangle_{tb} + |0_s 0_i\rangle_{tt} |1_s 1_i\rangle_{tb} \Big] \Big(1 - e^{(2\theta i)} \Big) +$$

$$+ \Big[|1_s 0_i\rangle_{tt} |0_s 1_i\rangle_{tb} + |0_s 1_i\rangle_{tt} |1_s 0_i\rangle_{tb} \Big] \Big(1 + e^{(2\theta i)} \Big)$$

If we take out and drop a global phase factor, we obtain:

$$|\psi_{out}\rangle = \sin(\theta) |\psi_{bunch}\rangle + i \cos(\theta) |\psi_{antibunch}\rangle \tag{4.5}$$

This is, aside from an unobservable i factor, the same result we obtained for a Mach-Zehnder and we report here for convenience the plot of the detection probabilities.
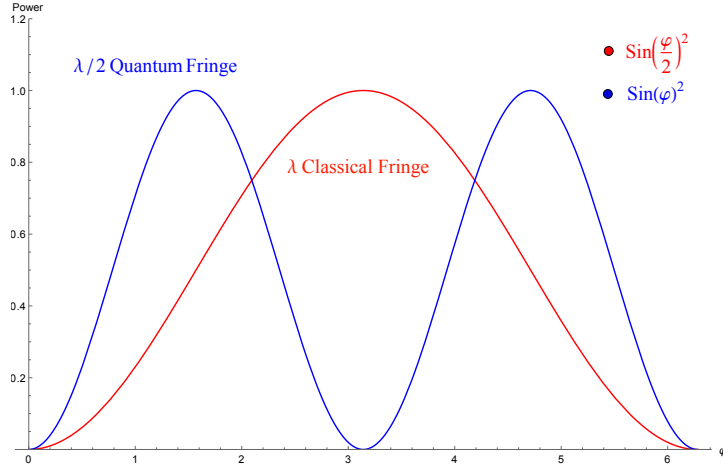
Figure 4.3: Classical and Quantum Interference.

After demonstrating the quality of the entanglement on Alice's chip, we need to prove the capability of our system to coherently transmit and distribute a Bell state. In order to do this, we replicate the scheme we consider before on Alice's side, but looking at the coincidences between port D1 and D3. Once again, we post select the signal and idler photon, respectively on port D1 and D3, with the aid of two off-chip DWDM. We can therefore neglect all the terms where the idler is in the top waveguides and the signal in the bottom ones. Furthermore, by looking at the detection coincidences, we can neglect the case where idler and signal are bunching and the state we have to consider is:

$$|\psi_{out}\rangle = \frac{1}{2\sqrt{2}}\,|1_s0_i\rangle_{tt}\,|0_s0_i\rangle_{tb}\,|0_s1_i\rangle_{bt}\,|0_s0_i\rangle_{bb} - e^{(2\theta i)}\,|0_s0_i\rangle_{tt}\,|1_s0_i\rangle_{tb}\,|0_s0_i\rangle_{bt}\,|0_s1_i\rangle_{bb}$$

We obtain this state with 25% (from here on we neglect the factor of 2 in the first fraction). We can rewrite this in the computational basis, with the convention that $|0\rangle$ maps to the cases $|1_s0_i\rangle_{tt}\,|0_s0_i\rangle_{tb}$ and $|0_s1_i\rangle_{bt}\,|0_s0_i\rangle_{bb}$, as:

$$|\psi_{out}\rangle = \frac{1}{\sqrt{2}}\Big(\,|0\rangle_{top}\,|0\rangle_{bottom} - e^{(2\theta i)}\,|1\rangle_{top}\,|1\rangle_{bottom}\,\Big) \qquad (4.6)$$

When we set θ to be equal to $\frac{\pi}{2}$ or π we obtain two Bell's state :

$$|\Phi_{\pm}\rangle = \frac{1}{\sqrt{2}}\Big(\,|0\rangle_{top}\,|0\rangle_{bottom} \pm |1\rangle_{top}\,|1\rangle_{bottom}\,\Big) \qquad (4.7)$$

We now apply the two projective operators $A\,(0,\phi_a)$ and $B\,(0,\phi_b)$ to the

state in the Fock basis (the result is the same for the logic basis but is somewhat less clearly understandable in terms of coincidence detection).

$$A\left(0, \phi_a\right) \otimes B\left(0, \phi_b\right)|\psi_{out}\rangle = \frac{1}{\sqrt{2}}\left[\left(a_{tt}^\dagger \sin\left(\frac{\phi a}{2}\right) + b_{tb}^\dagger \cos\left(\frac{\phi a}{2}\right)\right)\right.$$
$$\left(c_{bt}^\dagger \sin\left(\frac{\phi b}{2}\right) + d_{bb}^\dagger \cos\left(\frac{\phi b}{2}\right)\right) \pm \left(a_{tt}^\dagger \cos\left(\frac{\phi a}{2}\right) - b_{tb}^\dagger \sin\left(\frac{\phi a}{2}\right)\right)$$
$$\left.\left(c_{bt}^\dagger \cos\left(\frac{\phi b}{2}\right) - d_{bb}^\dagger \sin\left(\frac{\phi b}{2}\right)\right)\right]|vac\rangle$$

Let us consider $|\Phi_+\rangle$. If we factorize the products in the parentheses and apply the trigonometric identity for the difference of the angle $\phi a - \phi b$, we can write:

$$A\left(0, \phi_a\right) \otimes B\left(0, \phi_b\right)|\Phi_+\rangle =$$
$$= \frac{1}{\sqrt{2}}\left[\left(a_{tt}^\dagger c_{bt}^\dagger + b_{tb}^\dagger d_{bb}^\dagger\right)\cos\left(\frac{\phi a - \phi b}{2}\right) + \left(-b_{tb}^\dagger c_{bt}^\dagger + a_{tt}^\dagger d_{bb}^\dagger\right)\sin\left(\frac{\phi a - \phi b}{2}\right)\right]|vac\rangle =$$
$$= \frac{1}{\sqrt{2}}\left[\left(|1_s 0_i\rangle_{tt}|0_s 1_i\rangle_{bt} + |1_s 0_i\rangle_{tb}|0_s 1_i\rangle_{bb}\right)\cos\left(\frac{\phi a - \phi b}{2}\right) +\right.$$
$$\left.+ \left(|1_s 0_i\rangle_{tt}|0_s 1_i\rangle_{bb} - |1_s 0_i\rangle_{tb}|0_s 1_i\rangle_{bt}\right)\sin\left(\frac{\phi a - \phi b}{2}\right)\right]$$

After similar calculations for $|\Phi_-\rangle$ we can find:

$$A\left(0, \phi_a\right) \otimes B\left(0, \phi_b\right)|\Phi_-\rangle =$$
$$= \frac{1}{\sqrt{2}}\left[\left(-|1_s 0_i\rangle_{tt}|0_s 1_i\rangle_{bt} + |1_s 0_i\rangle_{tb}|0_s 1_i\rangle_{bb}\right)\cos\left(\frac{\phi a + \phi b}{2}\right) +\right.$$
$$\left.+ \left(|1_s 0_i\rangle_{tt}|0_s 1_i\rangle_{bb} + |1_s 0_i\rangle_{tb}|0_s 1_i\rangle_{bt}\right)\sin\left(\frac{\phi a + \phi b}{2}\right)\right]$$

The only factor which gives origin to a coincidence event (with our setup) is $|1_s 0_i\rangle_{tt}|0_s 1_i\rangle_{bt}$. We can therefore express the probability of detection with the following equations:

$$P(\Phi_+) \propto \cos^2\left(\frac{\phi a - \phi b}{2}\right)$$

$$P(\Phi_-) \propto \cos^2\left(\frac{\phi a + \phi b}{2}\right)$$

(4.8)

If we set ϕ_a to be $\left\{0, \frac{\pi}{2}, \pi, \frac{3\pi}{2}\right\}$ and scan ϕ_b continuously, we expect to see for different correlation fringes as shown in the Fig. 4.4.
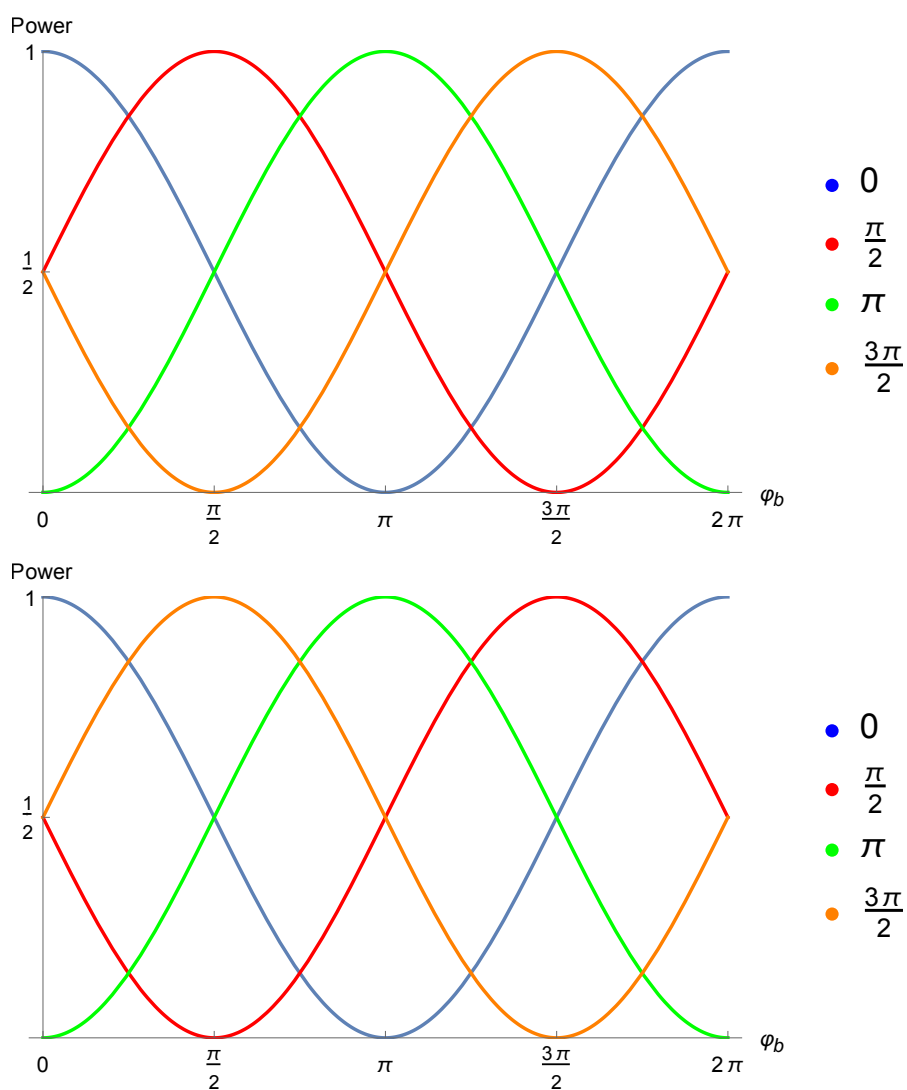
Figure 4.4: Correlations Fringes for the Bell states Φ_+ (up) and Φ_- (down)

Chapter 5

Characterization of the Components

5.1 Fabrication Details

The device we used for this experiment was fabricated using deep-UV lithography (193 nm) at LETI ePIXfab. The circuits were printed on a Silicon-on-Insulator wafer, with a 2 μm substrate of SiO_2 (silica) and a 220 nm silicon layer. The waveguide structures were 500 nm wide and fully etched (except those that made up the spiral sources, which were 470 nm wide see related section for further details). The nanometer scale of the waveguides is allowed by the very high refractive index of Si ($n_{Si} = 3.48$) compared to silica ($n_{Si} = 1.45$), which as a consequence enables the design of bending radii as small as 10 μm with close to negligible radiation loss (< 0.01 dB). As a result, the effective footprints of Alice's and Bob's chip are, respectively, of 1.2×0.5 mm^2 and 0.3×0.05 mm^2.

5.2 Optical Characterization of the Grating Couplers

Before moving to the full experiment we want to characterise the performance of the grating couplers in terms of loss and bandwidth. Optical access was achieved with an eight channels V-groove fibre array. The array was tilted 10° with respect to the normal axis of the chip in order to avoid a strong second order reflection back into the waveguide (see section 3.3). The 1D couplers were shallow etched, with a depth of 70 nm, and designed to have a period of 630 nm with a duty cycle of 0.5. The 2D grating couplers were also

shallow etched, with a period Λ of 630 nm and the diameters of the holes is 390 nm, while the full device has a footprint of 10 μm x 10 μm. The testing structure in Fig.5.1 were accessible on Alice's chip and we were therefore able to characterize the gratings independently.
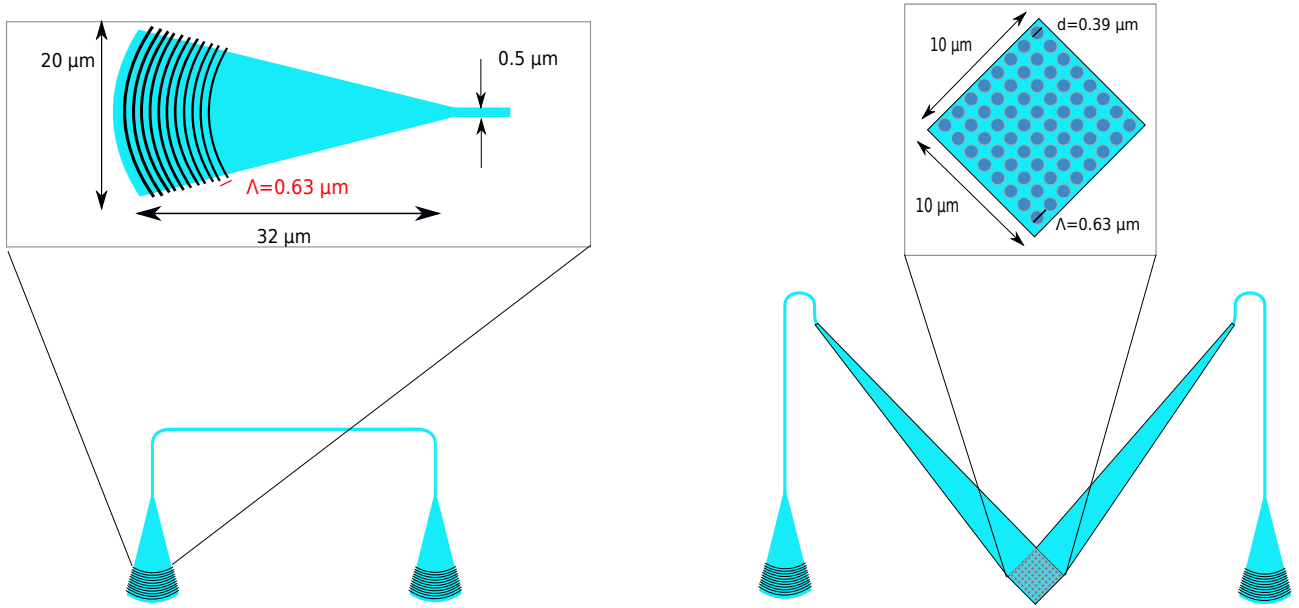

Figure 5.1: Testing structures for the grating couplers.

We recorded the transmitted power for each wavelength in the interval 1530-1580 (with a resolution of 0.1 nm) and we were able to reconstruct the transmission spectra of both 1D and 2D dimensional couplers, as shown in Fig. 5.2. For 1D gratings the excess loss measured was of -4.8 dB at peak wavelength, with a 1 dB bandwidth of 30 nm, as it is shown in Fig 5.2. 1D gratings are extremely sensible to polarization and only work for TE fields. The extinction ratio of TE with respect to TM modes was measured to be over 20 dB. For 2D gratings instead the measured excess loss was of -7.6 dB at the peak wavelength, with a 1 dB bandwidth of 30 nm.
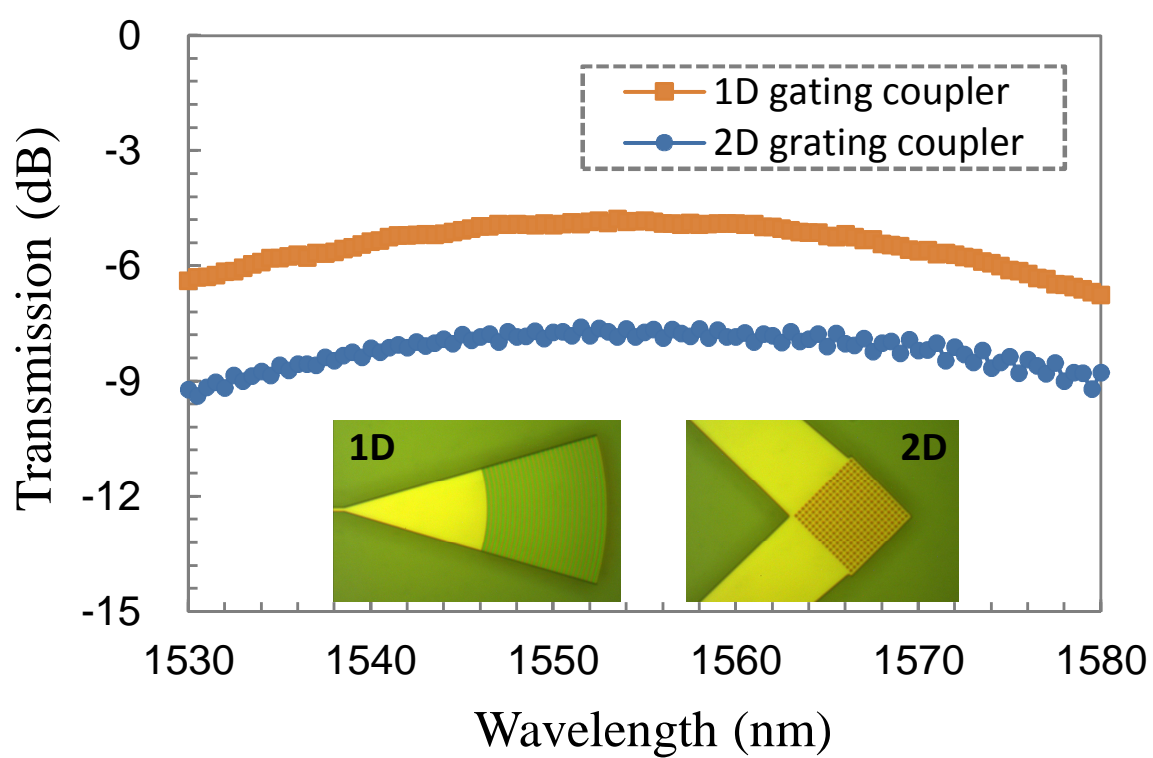
Figure 5.2: Spectrum of transmission of the 1D and 2D grating couplers.

5.3   Tomography Stage Characterisation

In order to finely tune the induced phase shift in the waveguide, we had to calibrate the thermal heaters, which were controlled by a homemade software interface. In order to do this, the optical power was recorded as a function of electrical power injected in the heater. A contour plot was obtained and fitted with least-squares minimization method. This method allows a reliable and direct map between the electrical power and the on chip projector. In Fig. 5.3 we show an example of such a plot with the corresponding states.
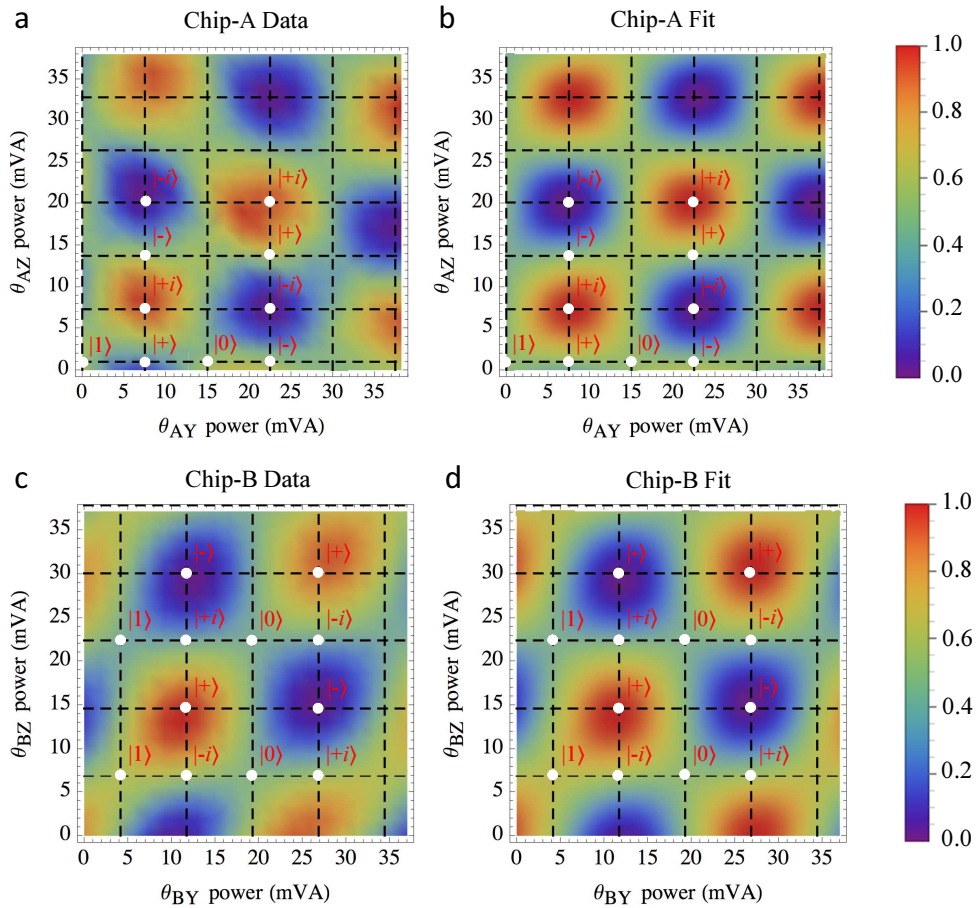

Figure 5.3: Contour Plot for $A(\theta_a, \phi_a)$ and $B(\theta_b, \phi_b)$

5.4   Path to Polarization Converter

An important feature of our experiment is the possibility of a coherent interconversion between path entangled and polarization entangled states by means of a 2D grating coupler. We rapidly repeat here the working principle while remanding to the relative section and to Bibliography for detailed information. A 2D grating coupler integrates the functionalities of a polarization beam splitter and a rotator for the TM mode. Randomly polarised light coupled into the grating will therefore be split into two nearly orthogonal waveguides, with a ratio proportional to the input state, whilst the TM component will also be rotated into a TE mode, more suitable for propagation into SoI devices. Randomly polarised light is proportionally mapped to either the top or the bottom waveguide. The final goal of our experiment is to convert a state encoded in path to polarization, send it through a fibre, reconvert it and then analyse it. In order to do this we must first characterise the fidelity of the conversion process. We therefore prepared a set of known polarization states with the help of a bulk tomography stage, shown in Fig 5.4, comprised of a polarization beam splitter, an half wave plate and a quarter wave plate.
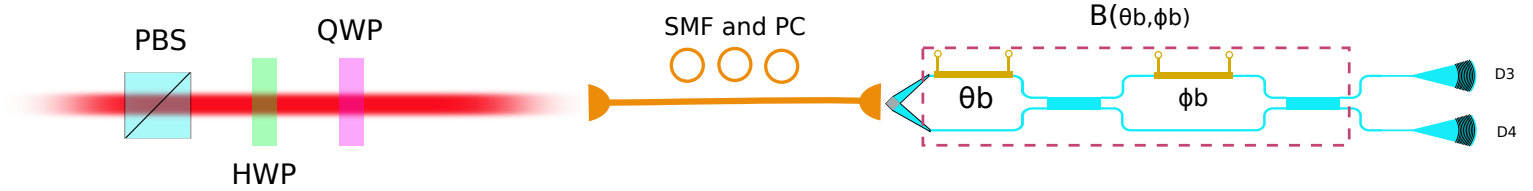

Figure 5.4: Experimental setup to characterise the PPC device.

The following six states were generated: $|H\rangle, |V\rangle, |D\rangle, |A\rangle, |R\rangle, |L\rangle$. With the help of a fibre and of a polarisation controller to compensate for random rotations of the fibre, the state was then coupled to the grating and analysed on chip with full state tomography technique. Fig. (5.5) shows a Bloch sphere representation of this process.

The quality of the conversion process was quantified by the following definition of fidelity:

$$F_{PPC} = \left(Tr \left[\sqrt{\sqrt{\rho_{pol}} \cdot \rho_{path} \sqrt{\rho_{pol}}} \right] \right)^2 \tag{5.1}$$

The fidelity obtained for each state is shown in Fig. (5.6), while the mean
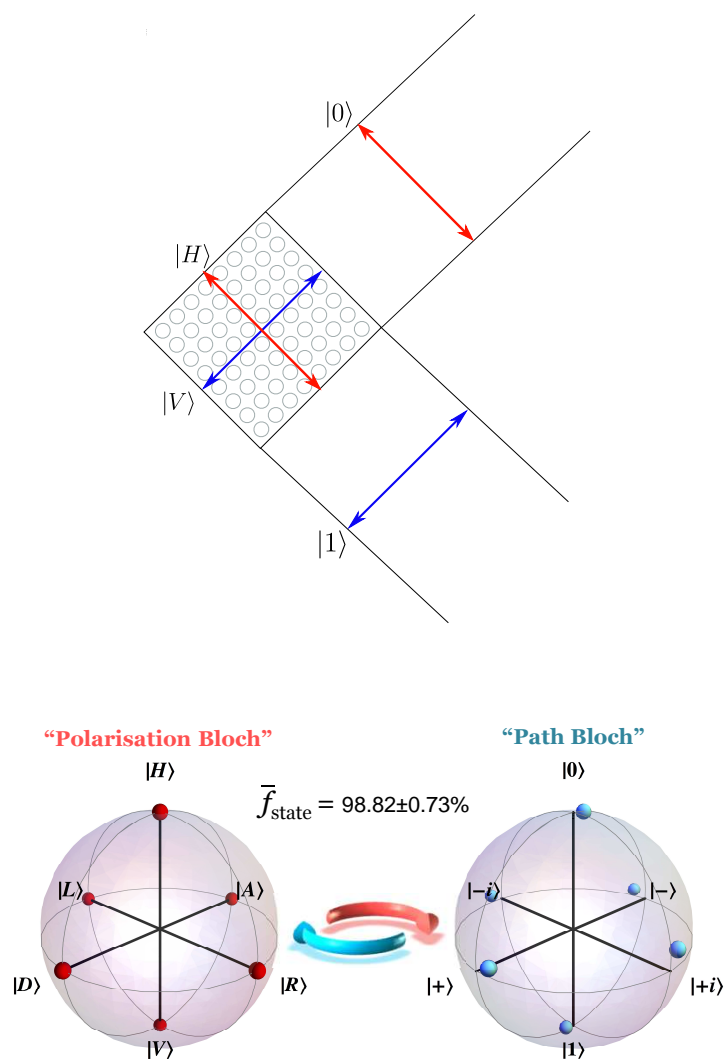
fidelity is $F_{PPC} = 98.82 \pm 0.73\%$.

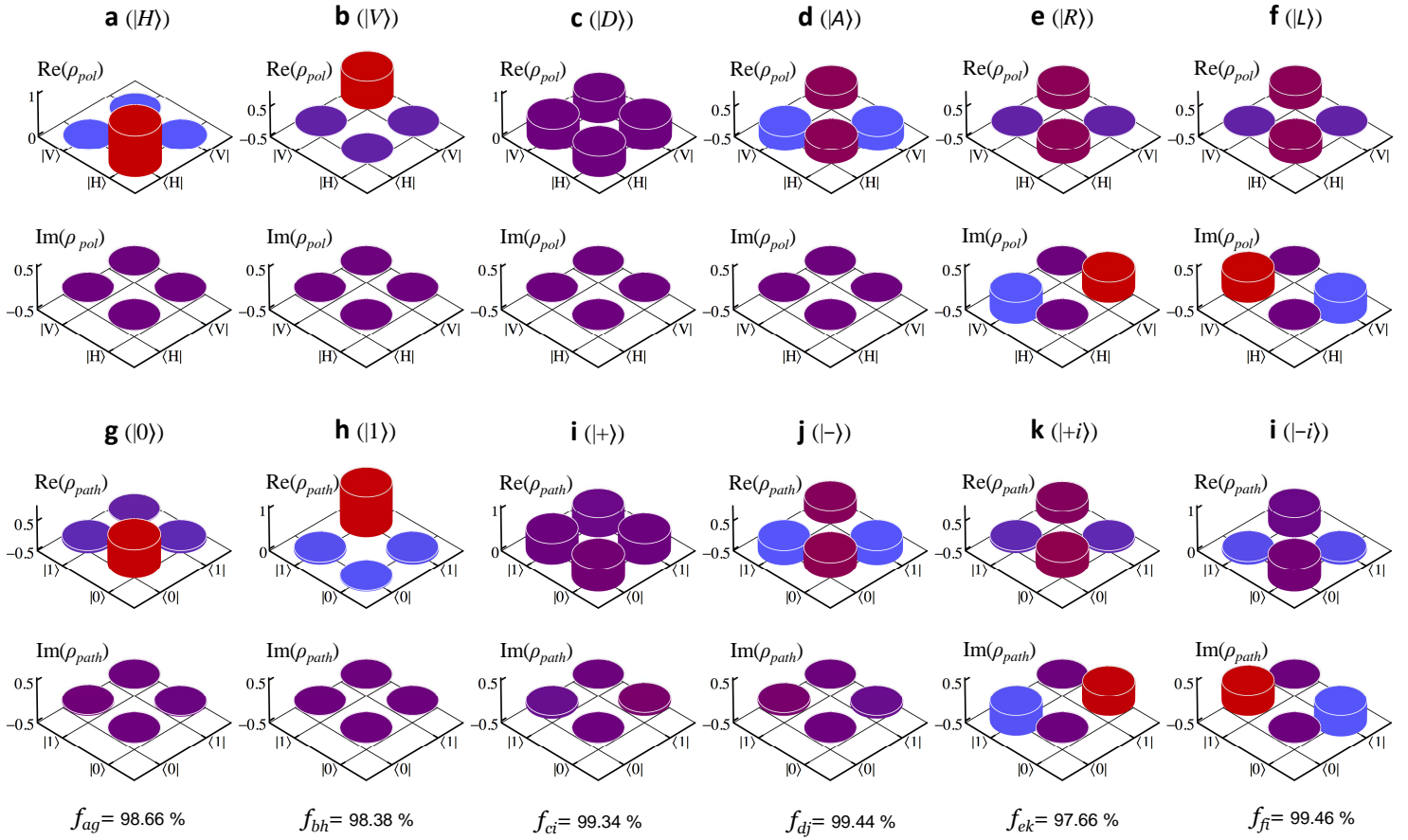Figure 5.5: Coherent map between polarization and entangled states on a Bloch sphere

Figure 5.6: (a)-(f). Ideal density matrix for the polarization encoded states. (g)-(i). Reconstructed density matrix of the path encoded states measured on chip. The corresponding state fidelities for each conversion are also listed.

Chapter 6

On Chip Generation of Entangled Qubits

6.1 On Chip Entanglement Generation

The next step was to verify the production of entangled states on Alice's chip. The visibility of quantum interference fringes, which we recorded as a function of θ (which was controlled by the source phase shifter, see Fig. 4.2), is a very well know parameter for the quality of the photon number entanglement. It is defined as follows:

$$V = 1 - \frac{N_{min}}{N_{max}} \tag{6.1}$$

Therefore we monitored the coincidence counts at port D1 and D2, since, as it was demonstrated in previous chapter, we expect to see a fringe with half the period when compared to classical light. The signal and idler photons were filtered before detection with the help of two DWDM. A 50 mW continuous way pump laser at 1555.5 nm was injected in the spiralled sources and a mean rate of $\sim 500 - 800$ Hz coincidences was recorded. The estimated efficiency of the SNSPDs was of 50% with ~ 800 Hz dark counts. The pump was also simultaneously recorded with a commercial power meter. The experimental results are shown in Fig. 6.1, where the classical fringe was self-normalized for clarity. We obtained an on chip visibility of $V_\lambda = 99.99 \pm 0.01\%$ for classical light and of $V_\lambda = 99.36 \pm 0.17\%$ for quantum interference. The accidental coincidences were subtracted and the error bar of each point was calculated assuming a poissonian statistics. The standard deviation of the mean visibility is instead calculated by a standard propagation error technique. The very high visibility occurs as a result of well

balanced MMI couplers and good spectral overlap between the two photon pair sources.
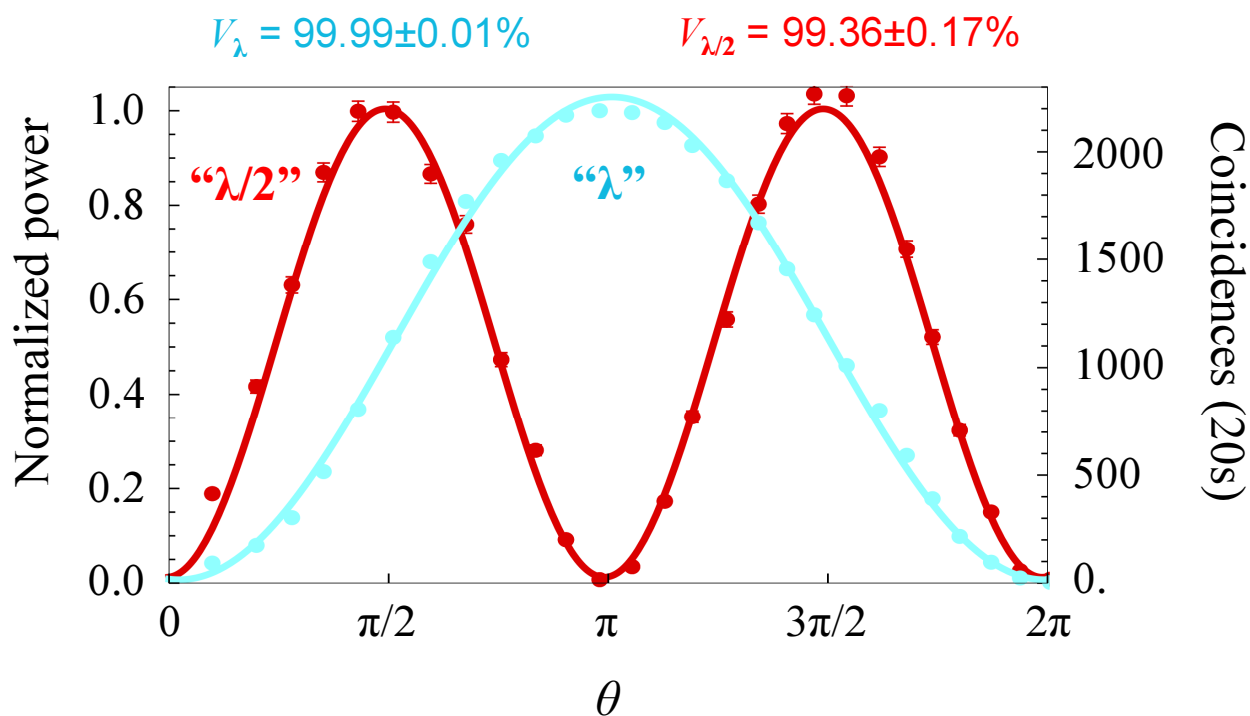

Figure 6.1: Experimental data for the classical and quantum interference.

Chapter 7

Entanglement Distribution between Two Chips

7.1 The Experimental Setup

The experimental setup used for demonstrating the distribution of the entanglement is shown in Fig.7.1. Bright light at the wavelength of 1555.5 nm, coming from a laser (Tunics-BT) with a tunable diode source (and a resolution of 10 pm), is amplified by an high power EDFA (Pritel with 30 dBm maximum power). The amplified spontaneous emission was suppressed with the aid of an off-chip DWDM (Openti). All the DWDMs used in this experiment had a 200 GHz channels spacing and a 1 nm 1 dB bandwidth. The bright light is then couple into the chip by means of an 8 channel, V-groove, single mode fibre array (OZ-Optics). The fibres were 127 μm apart and with a 10° angle with respect to the normal of the chip. A polarization controller was used to maximise the transmission through the grating coupler which supports only TE polarization. The on-chip sources, pump by coherent bright light, produce a path entangled state (via spontaneous four wave mixing) in two qubits. With the help of a 2D grating coupler we can coherently map the path entangled state to a polarization entangled state, send it through a 10 meters fibre, reconvert it by means of another 2D grating coupler and analyse it. A polarization controller allows us to compensate for random rotation of the polarization induced by the fibre. The temperature was controlled on both chips with a temperature controller (Thorlabs).Before detection, we filtered the signal and idler photons, on Alice's and Bob's side respectively, with two additional DWDM, using a channel 600 GHz away from the pump. The signal and idler photon were thus detuned of 4.8 nm from the pump. This way we could achieve an extinction ratio above 100

dB between our channels. Each DWDM introduces a 3 dB additional loss. Single photons were generated using superconducting nanowires single photon detectors (SNSPD) with an efficiency close to 50%. The coincidences events were then recorded by a time interval analyser (PicoHarp 300) with an integration window of 450 ps, which was chosen accordingly to the jitter time of the SNSPDs.

As it will be explained in the next sections, a rearranged version of the full setup was built during the different steps of the experiment, although, if not specified otherwise, the same basic components described here were used.
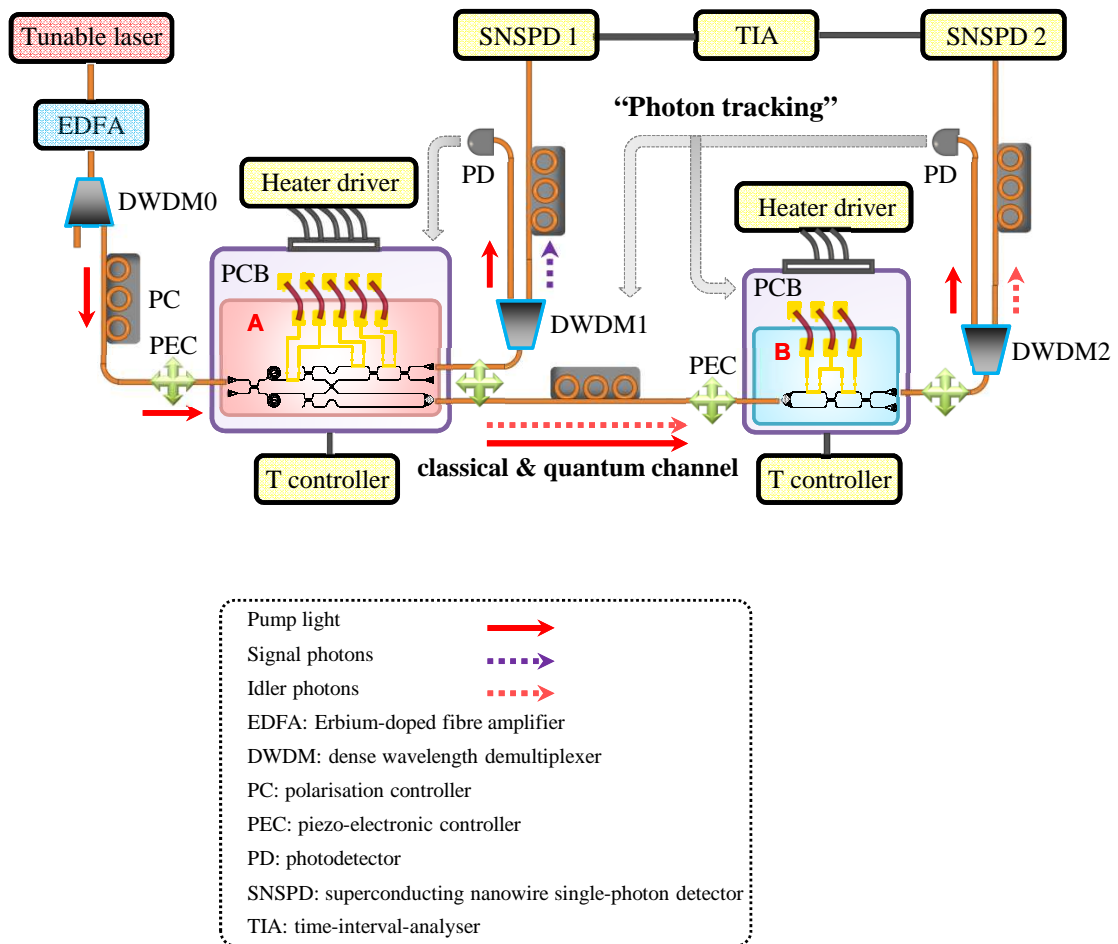

Figure 7.1: Full experimental apparatus

7.2 Correlation Fringes

We now turn our attention to the generation and detection of correlation fringes across the two chips. The photon number entangled state evolves to one of the two path entangled states $|\Phi_+\rangle$ or $|\Phi_-\rangle$ when the phase θ is set to $\frac{\pi}{2}$ or π. The entangled qubits were then separated and distributed between the two chips by means of the PPC interface. We simultaneously operate $A(0, \phi_a)$ and $B(0, \phi_b)$ in order to reproduce the theoretical outcome of Fig. 4.4, which is a consequence of Eq. 4.8:

$$P(\Phi_+) \propto \cos^2\left(\frac{\phi a - \phi b}{2}\right)$$

$$P(\Phi_-) \propto \cos^2\left(\frac{\phi a + \phi b}{2}\right)$$

We therefore fixed ϕ_a at the values $\left\{0, \frac{\pi}{2}, \pi, \frac{3\pi}{2}\right\}$ and scan ϕ_b continuously. The angles were choose in order to maximize the violation of the Bell's inequality in the CHSH form. The expected S parameter in this case is in fact related to the visibility of the fringes as follows[42]:

$$S_{fringes} = V\, 2\sqrt{2} \qquad (7.1)$$

It is apparent from the last formula that the critical visibility to violate the Bell's inequality is $V = \frac{1}{\sqrt{2}}$. The experimental results are shown in Fig. 7.2. A mean rate of 8-12 Hz was recorded after the two chips, while each point was integrated for 30 seconds. The fringes exhibit a mean visibility of $V_+ = 97.63 \pm 0.39\%$ and $V_- = 96.85 \pm 0.51\%$ respectively. Once again the accidental coincidences were subtracted and error bars were calculated assuming a Poissonian statistics. The estimated $S_{fringes}$, which is also the maximum achievable, is $S_+ = 2.761 \pm 0.011$ and $S_- = 2.739 \pm 0.015$.
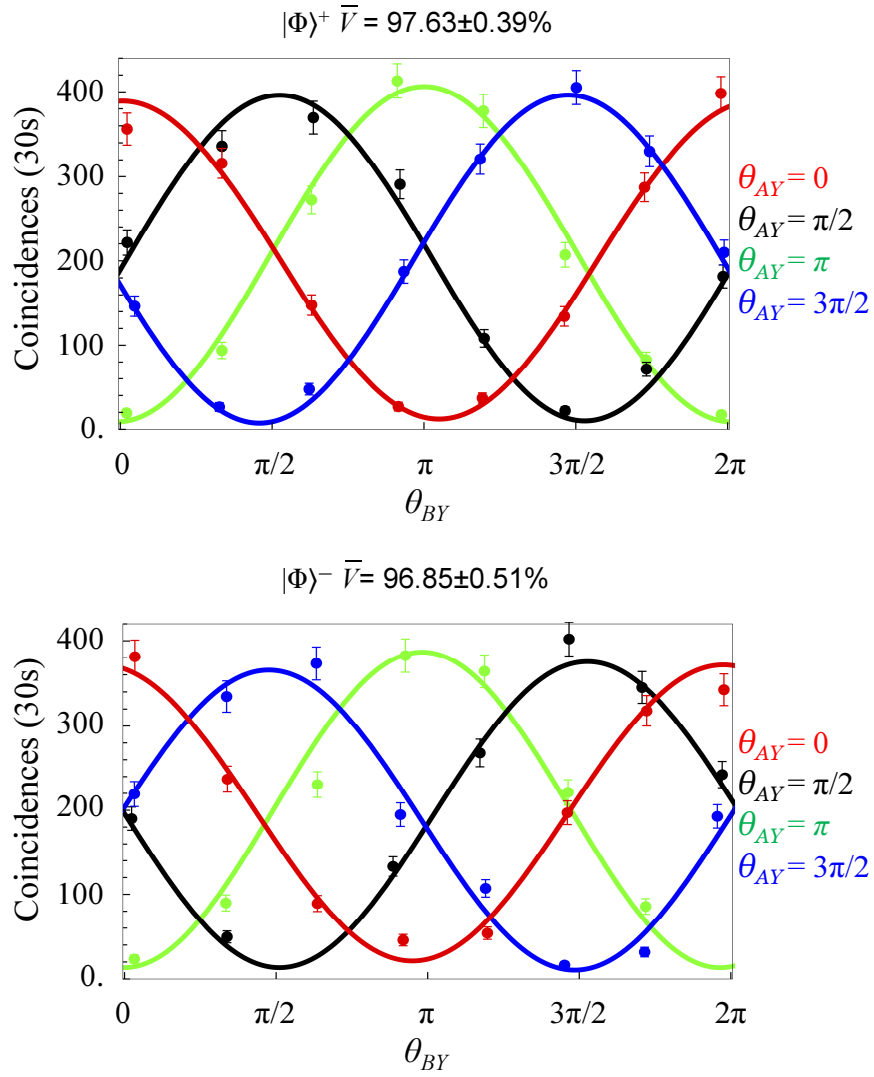
Figure 7.2: Correlation Fringes for different values of θ_a.

7.3 CHSH's Inequality Violation

The visibility of the correlation fringes is very high and the resulting $S_{fringes}$ parameter is very high[43, 44]. Notwithstanding, we want to confirm the distribution of entanglement with a rigorous and direct measurement of the CHSH inequality in the form:

$$S = |E\left(A_1, B_1\right) - E\left(A_2, B_2\right) + E\left(A_1, B_2\right) + E\left(A_2, B_1\right)| \leq 2 \qquad (7.2)$$

where $A_i = A\left(0, \phi_{ai}\right)$ with $\phi_{ai} \in \left\{0, \frac{\pi}{2}\right\}$ and $B_i = B\left(0, \phi_{bi}\right)$ with $\phi_{bi} \in \left\{\frac{\pi}{2}, \frac{3\pi}{4}\right\}$. The correlation coefficients are written in the form:

$$E\left(A_i, B_i\right) = \frac{C(\phi_{ai}, \phi_{bi}) + C(\phi_{ai} + \pi, \phi_{bi} + \pi) - C(\phi_{ai} + \pi, \phi_{bi}) - C(\phi_{ai}, \phi_{bi} + \pi)}{C(\phi_{ai}, \phi_{bi}) + C(\phi_{ai} + \pi, \phi_{bi} + \pi) + C(\phi_{ai} + \pi, \phi_{bi}) + C(\phi_{ai}, \phi_{bi} + \pi)}$$

As explained in the first chapter, the $C(C, \phi_{bi})$ are directly the coincidence obtained for the angles ϕ_{ai} and ϕ_{bi}) after an integration time of 60 seconds. As always, accidental coincidences are subtracted and the standard deviation is calculated from a Poissonian distribution. The values obtained for the different angles are listed in Fig. (7.3).
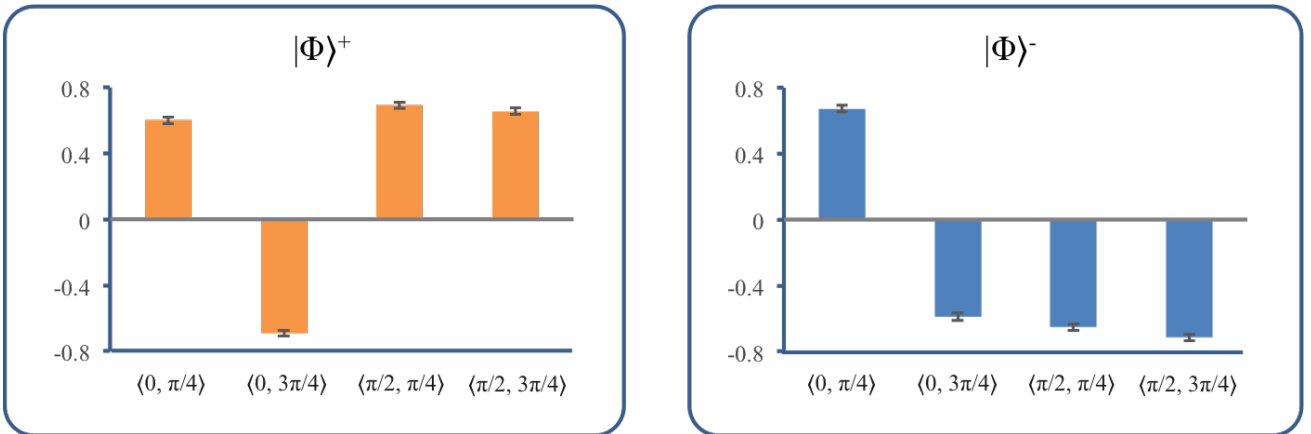

Figure 7.3: Histogram illustrating the correlation coefficients $E\left(A_i, B_i\right)$ for the various angles combination.

A straightforward application of (7.2) results in the parameters $S_+ = 2.638 \pm 0.039$ and $S_- = 2.628 \pm 0.041$ for the two Bell's state considered. These S_{CHSH} values violate the classical limit by 16.4 and 15.3 standard deviations, resulting in a strong confirmation of the entanglement distribution. The standard deviations are calculated assuming a Poissonian distribution of the single correlation coefficients. In Fig. 7.4 the experimental values of both the S numbers are shown, illustrating a good agreement.
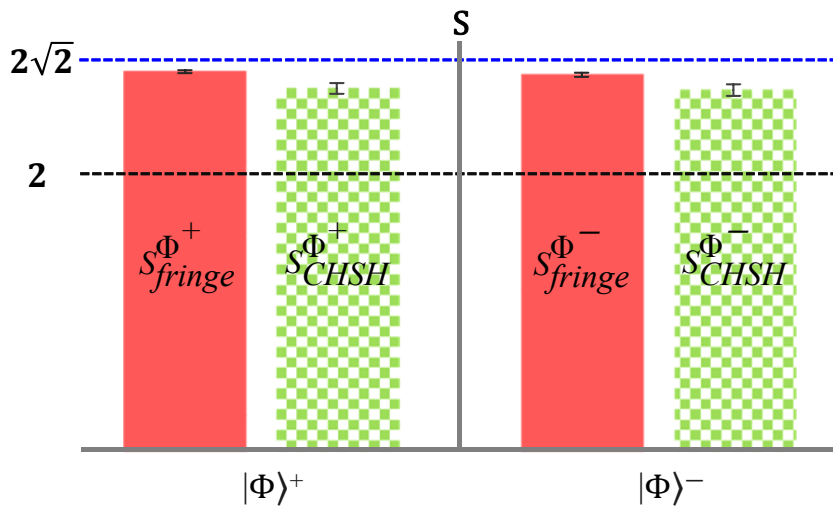

Figure 7.4: CHSH Violation

Chapter 8

Conclusions

We have successfully demonstrated the generation, manipulation and distribution of an entangled state between two integrated SoI chips. In fact, we firstly witnessed high visibility quantum interference, a clear mark of high quality photon-number entangled states. Secondly, we strongly violated Bell-CHSH inequality, confirming the distribution of entanglement across the two chips. Although in this experiment only 10 meters of single mode fibre were used, an arbitrary distance can separate the two chips, as long as decoherence can be neglected. A high fidelity polarization to path interconversion was also shown, demonstrating the potential of this device as a quantum photonic interconnect. Even though several challenges still remain, such as the considerably high loss of the system, or the design of an architecture suitable for many qubits distribution, this experiments confirms the importance of integrated silicon photonics for future real world quantum information applications.

Bibliography

[1] J. S. Bell, "On the einstein podolsky rosen", *Physics, 1, 195-200*, 1964.

[2] T. Ladd, F. Jelezko, R. Laflamme, Y. Nakamura, C. Monroe, and J. L. O'Brien, "Quantum computers", *Nature*, 2010.

[3] J. L. O'Brien, "Optical quantum computing", *Science*, 2007.

[4] J. L. O'Brien, A. Furusawa, and J. Vuckovic, "Photonic quantum technologies", *Nature Photonics*, 2009.

[5] E. Knill, R. Laflamme, and G. Milburn, "Efficient linear optics quantum computation", *Nature*, 2001.

[6] A. Politi, M. J. Cryan, J. G. Rarity, S. Yu, and J. L. O'Brien, "Silica-on-silicon waveguide quantum circuits", *Science*, 2008.

[7] A. Politi, J. C. F. Matthews, M. G. Thompson, , and J. L. O'Brien, "Integrated quantum photonics", *IEEE Journal of Selected Topics in Quantum ELectronics*, 2009.

[8] M. Thompson, A. Politi, J. Matthews, and J. O'Brien, "Integrated waveguide circuits for optical quantum computing", *The Institution of Engineering and Technology*, 2011.

[9] A. Peruzzo, M. Lobino, J. C. F. Matthews, N. Matsuda, A. Politi, K. Poulios, X.-Q. Zhou, Y. Lahini, N. Ismail, K. Wrhoff, Y. Bromberg, Y. Silberberg, M. G. Thompson, and J. L. OBrien, "Quantum walks of correlated photons", *Science*, 2010.

[10] J. Carolan, C. Harrold, C. Sparrow, E. Martn-Lopez, N. J. Russell, J. W. Silverstone, P. J. Shadbolt, N. Matsuda, M. Oguma, M. Itoh, G. D. Marshall, M. G. Thompson, J. C. F. Matthews, T. Hashimoto, J. L. OBrien, and A. Laing, "Universal linear optics". ArXiv, 2015.

[11] P. J. Shadbolt, M. R. Verde, A. Peruzzo, A. Politi, A. Laing, M. Lobino, J. C. F. Matthews, M. G. Thompson, and J. L. OBrien, "Generating, manipulating and measuring entanglement and mixture with a reconfigurable photonic circuit", *Nature Photonics*, 2011.

[12] D. Bonneau, M. Lobino, P. Jiang, C. M. Natarajan, M. G. Tanner, R. H. Hadfield, S. N. Dorenbos, V. Zwiller, M. G. Thompson, and J. L. OBrien, "Fast path and polarization manipulation of telecomwavelength single photons in lithium niobatewaveguide devices", *Physical Review Letters*, 2012.

[13] J. W. Silverstone, D. Bonneau, K. Ohira, N. Suzuki, H. Yoshida, N. Iizuka, M. Ezaki, C. M. Natarajan, M. G. Tanner, R. H. Hadfield, V. Zwiller, G. D. Marshall, J. G. Rarity, J. L. OBrien, and M. G. Thompson, "On-chip quantum interference between silicon photon-pair sources", *Nature Photonics*, 2013.

[14] X.-S. Ma, T. Herbst, T. Scheidl, DaqingWang, S. Kropatschek, W. Naylor, B. Wittmann, A. Mech, J. Kofler, E. Anisimova, V. Makarov, T. Jennewein, R. Ursin, and A. Zeilinger, "Quantum teleportation over 143 kilometres using active feed-forward", *Nature*, 2012.

[15] J. Yin, J.-G. Ren, H. Lu, Y. Cao, H.-L. Yong, Yu-PingWu, C. Liu, S.-K. Liao, F. Zhou, Y. Jiang, X.-D. Cai, P. Xu, G.-S. Pan, J.-J. Jia, Y.-M. Huang, H. Yin, J.-Y. Wang, Y.-A. Chen, C.-Z. Peng, and J.-W. Pan, "Quantum teleportation and entanglement distribution over 100-kilometre free-space channels", *Nature*, 2012.

[16] R. Ursin, F. Tiefenbacher, T. S.-M. H. Weier, T. Scheidl, M. Lindenthall, B. Blauensteiner, T. Jennewein, J. Perdigues, P. Trojekt, B. Omer, M. Furst, M. Meyenburg, J.Rarity, Z. Sodnik, C. Barbieri, H. Weinfurter, and A. Zeilenger, "Entanglement-based quantum communication over 144km", *Nature Physics*, 2007.

[17] M. A. Nielsen and I. L. Chuang, *Quantum Computation and Quantum Information*. Cambridge University Press, 2010.

[18] C. P. WIlliams, *Explorations in Quantum Computing*. Springer, 2011.

[19] D. Bonneau, *Integrated quantum photonics at telecommunication wavelength in silicon-on-insulator and lithium niobate platforms*. PhD thesis, University of Bristol, 2013.

[20] S. M. Barnett and P. M. Radmore, *Methods in Theoretical Quantum Optics.* Oxford University Press, 2002.

[21] L. Mandel and E. Wolf, *Optical Coherence and Quantum Optics.* Cambridge University Press, 1995.

[22] X. Y. Zou, L. J. Wang, and L. Mandel, "Induced coherence and indistinguishability in optical interference", *Physical Review Letters*, 1991.

[23] C. K. Hong, Z. Y. Ou, and L. Mandel, "Measurement of subpicosecond time intervals between two photons by interference", *Physical Review Letters*, 1987.

[24] A. Einstein, B. Podolsky, and N. Rosen, "Can quantum-mechanical description of physical reality be considered complete?", *Physical Review*, 1935.

[25] J. F. Clauser, M. A. Horne, A. Shimony, and R. A. Holt, "Proposed experiment to test local hidden-variable theories.", *Physical Review Letters*, 1969.

[26] A. Aspect, "Bells inequality test: more ideal than ever", *Nature*, 1999.

[27] J.S.Bell, *Speakable and Unspeakable in Quantum Mechanics.* Cambridge University Press, 2004.

[28] D. F. V. James, P. G. Kwiat, W. J. Munro, and A. G. White, "Measurements of qubits", *Physical Review A*, 2001.

[29] J. B. Altepeter, D. F. V. James, and P. G. Kwiat, *Quantum State Tomography.*

[30] M. D. de Burgh, N. K. Langford, A. C. Doherty, and A. Gilchrist, "Choice of measurement sets in qubit tomography", *Physical Review*, 2008.

[31] L. Pavesi and D. J. Lockwood, *Silicon Photonics.* Springer, 2003.

[32] S. Photonics, *Silicon Photonics II.* Springer, 2011.

[33] L. B. Soldano and E. C. M. Pennings, "Optical multi-mode interference devices based on self-imaging : Principles and applications", *Journal of Lightwave Technology*, 1995.

[34] D. Taillaert, F. V. Laere, M. Ayre, W. Bogaerts, D. V. Thourhout, P. Bienstman, and R. Baets, "Grating couplers for coupling between optical fibers and nanophotonic waveguides", *Japanese Journal of Applied Physics*, 2006.

[35] F. V. Laere, T. Claes, J. Schrauwen, S. Scheerlinck, M. Wim Bogaerts, D. Taillaert, L. OFaolain, D. V. Thourhout, and R. Baets, "Compact focusing grating couplers for silicon-on-insulator integrated circuits", *IEEE Photonics Technology Letters*, 2007.

[36] D. Taillaert, P. Bienstman, and R. Baets, "Compact efficient broadband grating coupler for silicon-on-insulator waveguides", *Optical Society of America*, 2004.

[37] D. Taillaert, H. Chong, P. I. Borel, L. H. Frandsen, R. M. D. L. Rue, and R. Baets, "A compact two-dimensional grating coupler used as a polarization splitter", *IEEE Photonics Technology Letters*, 2003.

[38] Z. Yang, M. Liscidini, and J. E. Sipe, "Spontaneous parametric down-conversion in waveguides: A backward heisenberg picture approach", *Physical Review A*, 2008.

[39] M. Liscidini, L. Helt, and J. E. Sipe, "Asymptotic fields for a hamiltonian treatment of nonlinear electromagnetic phenomena", *Physical Review A*, 2012.

[40] J. C. F. Matthews, A. Politi, A. Stefanov, and J. L. OBrien, "Manipulation of multiphoton entanglement in waveguide quantum circuits", *Nature Photonics*, 2009.

[41] M. Reck and A. Zeilinger, "Experimental realization of any discrete unitary operator", *Physical Review Letters*, 1994.

[42] J. G. Rarity and P. R. Tapster, "Experimental violation of bell's inequality based on phase and momentum", *Physical Review Letters*, 1990.

[43] A. Aspect, P. Grangier, and G. Roger, "Experimental realization of einstein-podolsky-rosen-bohm gedankenexperiment: A new violation of bell's inequalities", *Physical Review Letters*, 1982.

[44] A. Aspect, J. Dalibard, and G. Roger, "Experimental test of bell's inequalities using time-varying analyzers", *Physical Review Letters*, 1982.